Volume 16
Number 22
14 June 2025
Pages 2567-2694

Polymer Chemistry

rsc.li/polymers

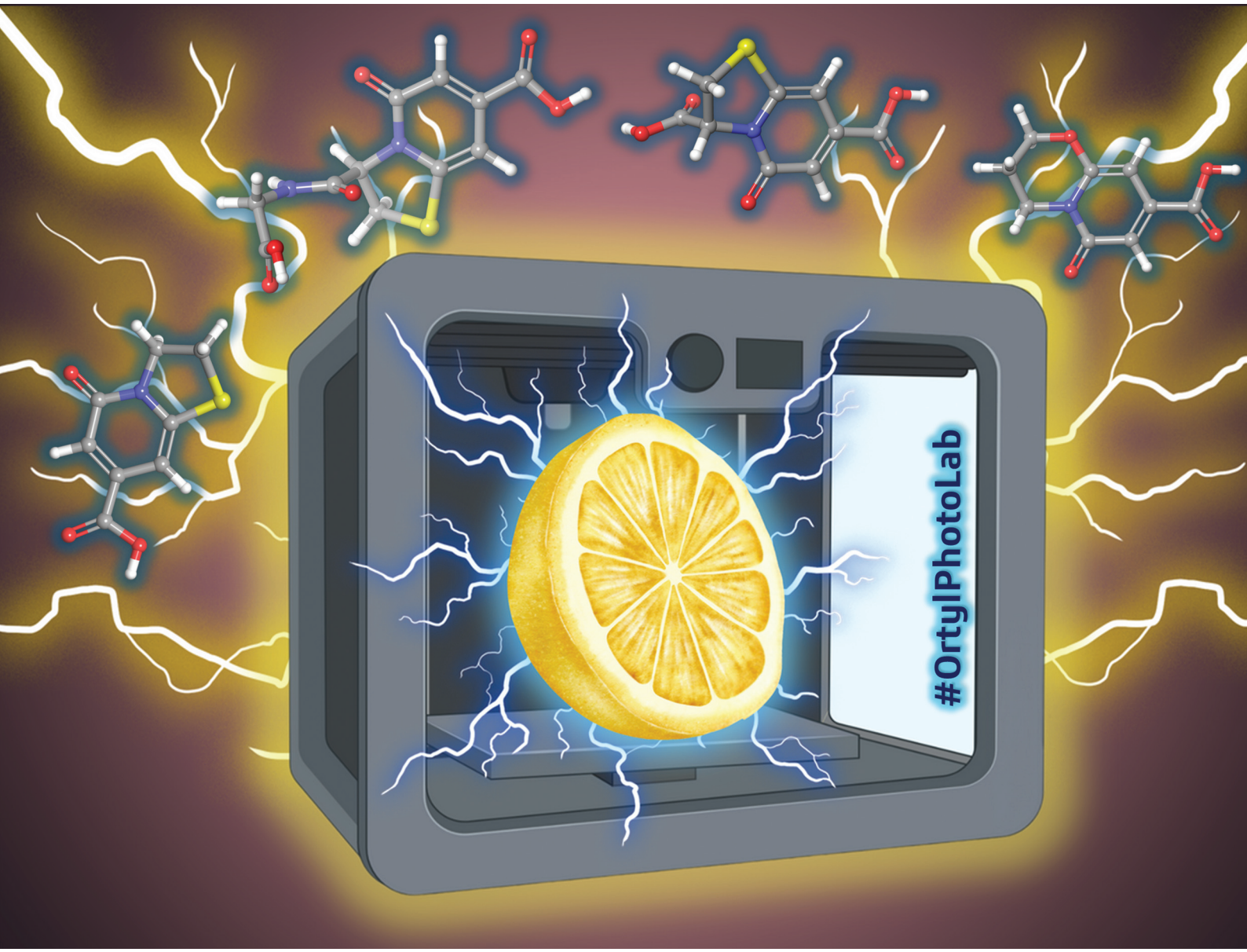

ISSN 1759-9962

ROYAL SOCIETY OF CHEMISTRY

PAPER
Joanna Ortyl *et al.*
Effective photoinitiating systems using citric acid-derived chromophores as photosensitizers for 3D bio-printing applications

15 YEARS ANNIVERSARY

Polymer Chemistry

ROYAL SOCIETY OF CHEMISTRY

PAPER

View Article Online
View Journal | View Issue

Cite this: *Polym. Chem.*, 2025, **16**, 2580

Effective photoinitiating systems using citric acid-derived chromophores as photosensitizers for 3D bio-printing applications†

Katarzyna Starzak,[a,b] Alicja Wysocka,[a,b] Łukasz Waluda,[a,b] Patryk Szymaszek,[a,b] Wiktor Kasprzyk[a] and Joanna Ortyl *[a,c,d]

The growing interest in the use of naturally derived compounds, associated with the increasing focus on green chemistry principles in various fields of chemical technology, is also evident in the development of light-cured resins for 3D printing. Therefore, in this work, four fluorophores formed alongside carbon dots as one of the products of the reaction between citric acid and specific β-amines were comprehensively studied. These studies facilitated the detailed optical characterization of the compounds, which in turn led to a better understanding of the electron transfer mechanisms accompanying the initiation of photopolymerization processes. In addition, cyclic voltammetry and photostability studies enabled a preliminary assessment of the applicability of the fluorophores as photosensitizers of commercially available diphenyl iodonium salts (SpeedCure 938®). FT-IR analyses and supporting photorheology measurements made it possible to determine the kinetics of the photopolymerization process and demonstrate the influence of the water content (non-reactive agent) on its course. Finally, it was possible to develop resins for 3D printing with low viscosity for use in the stereolithography (SLA) method and high viscosity for use in the direct ink writing (DIW) method enriched with light-curing of the finished pattern.

Received 9th December 2024,
Accepted 21st March 2025

DOI: 10.1039/d4py01409j

rsc.li/polymers

1. Introduction

Photopolymerization is revolutionizing the way we approach the production of polymer materials, offering innovative solutions across various industries. This dynamic process enables the transformation of monomers and oligomers into solid polymers upon exposure to light, which is driven by the action of photoinitiators. This process takes place using photoinitiators that absorb light and generate reactive molecules or free radicals, which are responsible for the initiation of the polymerization process.[1–4] Photopolymerization is characterized by a fast curing time, which allows fast production processes.[5,6] It is also an easily controllable process, as the curing time can be controlled by adjusting the parameters of the light sources used, such as light intensity, wavelength, and exposure time.[7–9] Radical photopolymerization is a process in which photoinitiators generate radicals, which in turn initiate polymerization reactions.[10–12] In this process, the photoinitiator undergoes photodegradation upon light exposure and transitions from the ground state to the excited state.[13,14] In radical photopolymerization, photoinitiators generate reactive radicals that are highly reactive and initiate polymerization reactions, combining with monomers to form polymer chains.[15–17] Nowadays, photopolymerization processes are widely used in industry, including the production of protective coatings,[18–20] paints,[21,22] adhesives,[23–25] dental materials,[26,27] medicine,[28–30] electronics,[31–33] architecture,[34,35] as well as in 3D printing.[36–40]

The latter process is based on the principle of additive manufacturing, that is, objects are created by applying successive layers of material on top of each other, rather than through traditional material removal methods such as CNC machining.[41,42] The use of naturally derived compounds in chemistry and chemical technology is important for both environmental protection and development of new and sustainable production methods.[43–47] Another important aspect is the wide spectrum of applications of natural compounds. In organic chemistry, compounds of natural origin are often used as raw materials for organic synthesis, making it possible to obtain a variety of chemical products. Natural compounds

[a]*Department of Biotechnology and Physical Chemistry, Faculty of Chemical Engineering and Technology, Cracow University of Technology, Warszawska 24, Cracow, 31-155, Poland. E-mail: jortyl@pk.edu.pl*
[b]*CUT Doctoral School, Faculty of Chemical Engineering and Technology, Cracow University of Technology, Warszawska 24, Cracow, 31-155, Poland*
[c]*Photo HiTech Ltd, Bobrzyńskiego 14, 30-348 Cracow, Poland*
[d]*Photo4Chem Ltd, Lea 114, 30-133 Cracow, Poland*

† Electronic supplementary information (ESI) available. See DOI: https://doi.org/10.1039/d4py01409j

have applications in the production of biodegradable materials such as polymers and can replace traditional plastics.[44,48] In addition, natural dyes can be used as sources of interesting photoactive compounds that cover almost the entire range of visible and ultraviolet light.[49,50]

The synthesis of fluorescent materials from natural sources, such as citric acid, has recently gained much interest, mainly because of the low cost of their synthesis and high photoluminescence (PL) quantum yield.[51–55] Fluorophores obtained using citric acid and other natural compounds have been widely applied in various fields.[56] They are used as pH sensors,[57–59] biomarkers,[60–62] fluorescent inks,[63–65] materials for solar cells,[63,66] fluorescent probes for detection of different ions and molecules,[67–71] and fluorescent tracers for monitoring various processes.[72] Owing to their favorable physicochemical properties and biocompatibility, they have great potential for further development and widespread use in chemistry and chemical technology.[73] As has been proven before, the products of synthesis, including citric acid as one of the key substrates, can be used as photosensitizers in initiating systems dedicated to light-induced polymerization processes.[74]

Taking into account all the above-mentioned dependences and factors, it is necessary to further develop safe photosensitizers that absorb electromagnetic radiation from the visible range. Therefore, the development of initiating systems based on fluorophores derived from the synthesis of carbon dots from citric acid as the main precursor of the tested compounds was undertaken for the first time as this has never been investigated before. Studied compounds except for their performance as photosensitizers also exhibit excellent water solubility greater than some of the most common components of photoinitiating systems of natural origin such as: riboflavin which is soluble in water only to a limited extent or curcumin that doesn't exhibit any solubility in aqueous media. Within the framework of this study, a series of analyses was carried out on the application of four fluorophores synthesized from citric acid and specific β-amines for free-radical photopolymerization processes. Spectroscopic studies provided information about the optical characteristics of the studied compounds, while electrochemical studies and thermodynamic calculations made it possible to determine the potential use of fluorophores for specific two- and three-component initiating systems dedicated to free-radical photopolymerization. The efficiency of the tested initiating systems was confirmed using real-time Fourier-transform infrared spectroscopy (real-time FTIR). Photorheological studies were used as an additional method to study the kinetics of photopolymerization processes and the suitability of the developed compositions for use in 3D printing processes. Additionally, the effects of different water contents (non-reactive components) on the kinetics of the process and the final conversion were studied. However, it also allows the determination of the properties of polymeric materials obtained by this method, such as polymerization shrinkage. The last stage of this research was to make 3D prints using two different techniques, stereolithography (SLA) and direct ink writing (DIW), for the compositions selected on the basis of the aforementioned studies.

2. Materials and methods

2.1. Materials

A series of four citric acid-derived fluorophores, namely 5-oxo-2,3-dihydro-5*H*-[1,3]thiazolo[3,2-*a*]pyridine-7-carboxylic acid (**CCA**), 5-oxo-2,3-dihydro-5*H*-[1,3]thiazolo[3,2-*a*]pyridine-3,7-dicarboxylic acid (**TPA**), 6-oxo-3,4-dihydro-2*H*,6*H*-pyrido[2,1-*b*][1,3]oxazine-8-carboxylic acid (**ODPC**), and 3-[(carboxymethyl)carbamoyl]-5-oxo-2,3-dihydro-5*H*-[1,3]thiazolo[3,2-*a*]pyridine-7-carboxylic acid (**CTPC**) (Fig. 1), were synthesized according to the description given in the ESI.† The applicability of the obtained fluorophores as iodonium salt photosensitizers for free-radical photopolymerization was assessed using the numerous methods described in the following subsections. The synthetic procedures for the tested compounds, along with structural characterization performed using NMR and LCMS methods, are presented in the ESI.†

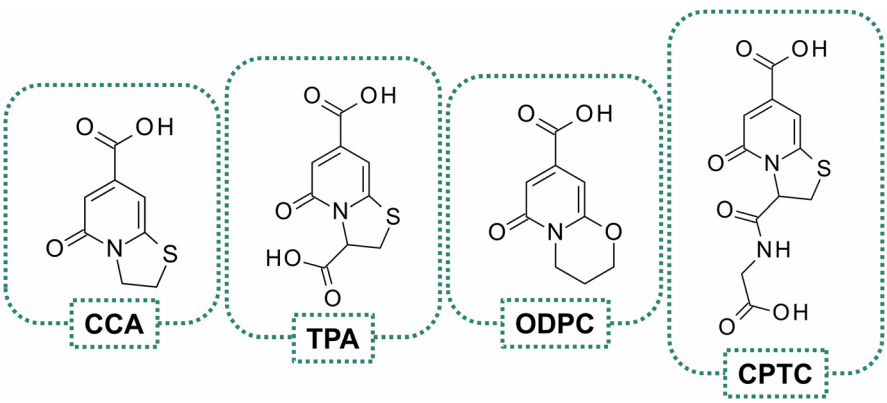

Fig. 1 Structures of citric acid derived fluorophores investigated in this study.

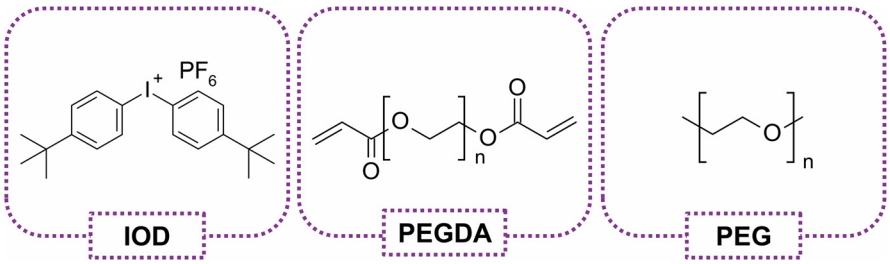

Fig. 2 Corresponding structures of photoinitiator, reactive part (**PEGDA** M_n = 700 g mol^{-1}) and non-reactive part (**PEG** M_n = 2000 g mol^{-1}) used in this study.

The photoinitiating system consisted of bis(4-*t*-butylphenyl) iodonium hexafluorophosphate (**IOD**, from Lambson) as a model photoinitiator sensitized by the studied compounds. Poly(ethylene glycol)diacrylate with a number-average molar mass of M_n = 700 g mol^{-1} (**PEGDA**, from Sigma Aldrich) was used as the reactive component. Poly(ethylene glycol) (**PEG**), with a number-average molar mass of M_n = 2000 g mol^{-1} was also used in certain compositions. The corresponding structures of all compounds used are shown in Fig. 2. Additionally, water was used as a non-reactive compound, and its influence on the entire process was studied.

2.2. UV-VIS absorption and photoluminescence characteristics

The UV-VIS absorption spectra of the studied derivatives in acetonitrile and distilled water were collected using a Cary 60 UV-Vis spectrophotometer (Agilent, Santa Clara, CA, USA) with a spectral range of 190–1100 nm. The tests were performed at 25 °C in the range 200–800 nm in a quartz cuvette with an optical path of 10 mm.

A FluoroMax-4P spectrofluorometer (Horiba, Kyoto, Japan) was used to obtain PL emission and excitation spectra of the studied compounds. Measurements were conducted using a quartz cuvette with an optical pathway of 10 mm. All PL spectra were obtained using specific excitation and emission wavelengths and plotted within an appropriate range (the specific volumes of PL λ_{ex} and PL λ_{em} and the spectral range are depicted in the corresponding figures).

2.3. Electrochemical determination of oxidation and reduction potential

Electrochemical analyses were performed to determine the oxidation (E_{ox} against Ag/AgCl) and reduction potentials (E_{red} *vs.* Ag/AgCl) of the studied fluorophores using cyclic voltammetry carried out using an electrochemical Analyzer M161 and Electrode Stand M164 (from MTM-ANKO, Poland). Tetrabutylammonium hexafluorophosphate (0.1 M) (from Sigma Aldrich) was employed as supporting electrolyte, a silver chloride electrode was made as reference (Ag/AgCl) while platinum disc was used as a working electrode. A scan rate of 0.1 V s^{-1} was utilized, and potentials were calculated using half peak potentials. Ferrocene was used as a reference. Gibbs free energy ΔG_{et} calculations for the electron transfer process between the components of the initiating system were performed from the resulting oxidation and reduction potentials using the following eqn (1):

$$\Delta G_{et} = F\left[E_{ox} \cdot \frac{D}{D^{\bullet+}} - E_{red} \cdot \frac{A^{\bullet-}}{A}\right] - E_{00} - \frac{Ze^2}{\varepsilon a} \quad (1)$$

where E_{ox} ($D/D^{\bullet+}$) is the oxidation potential of the electron donor, E_{red} ($A^{\bullet-}/A$) is the electron acceptor reduction potential, E_{00} is the energy of the excited state, $(Ze^2/\varepsilon a)$ – the electrostatic energy of the interaction between the initially formed ion pair. For polar solvents, the $(Ze^2/\varepsilon a)$ parameter can be neglected. The energy of the excited state was determined from the excitation and emission spectra obtained *via* measurements using a FluoroMax-4P spectrofluorometer (Horiba, Kyoto, Japan).

2.4 Determination of average fluorescence lifetimes

The average fluorescence lifetimes of the fluorophores were measured using a time-correlated single-photon counting system (TCSPC) DeltaFlex™ (Horiba, Kyoto, Japan). The experiments were conducted using solutions of the fluorophores in acetonitrile and distilled water. The samples were excited at 369 nm, and data were collected for wavelengths corresponding to the maximum emission spectrum of each derivative. Measurements were performed in a quartz cuvette with an optical path of 10 mm at a constant temperature of 25 °C. An aqueous solution of Ludox (Sigma Aldrich) was used as a reference for all measurements.

2.5. Fluorescence quenching and mechanism of electron transfer from the excited state

To investigate the changes in the PL emission spectra of the citric acid-based fluorophores in acetonitrile, a FluoroMax-4P spectrofluorometer (Horiba, Kyoto, Japan) was used. Experiments were performed using **IOD** as a fluorescence-quenching agent for the investigated compounds. This study involved the determination of PL changes in the intensity of the emission spectrum of the tested derivatives with the concentration of the quenching agent. Tests were performed at 25 °C in a quartz cuvette with an optical path length of 10 mm. The excitation wavelength was chosen individually for all fluorophores considering the maximum excitation spectra.

Fluorescence quenching measurements enabled the determination of the electron transfer constant between the photo-

sensitizer in the excited state and diphenyliodonium salt. The electron transfer constant (k_q) was determined using the Stern–Volmer equation:

$$\frac{I_0}{I} = 1 + K_{SV}[\mathbf{IOD}] = 1 + k_q\tau_0[\mathbf{IOD}] \quad (2)$$

where I_0 is the fluorescence intensity of the photosensitizer in the absence of the fluorescence quencher, I is the fluorescence intensity of the photosensitizer in the presence of the fluorescence quencher, and τ_0 is the excited-state lifetime of the photosensitizer in the absence of the fluorescence quencher.

The quantum yield of the electron transfer from the excited state ($\Phi_{et(S1)}$) was calculated using the following equation:

$$\Phi_{et(S1)} = \frac{K_{SV}[\mathbf{IOD}]}{1 + K_{SV}[\mathbf{IOD}]}. \quad (3)$$

2.6. Steady state photolysis of citric acid derived fluorophores

Photolysis measurements were performed for all the fluorophores in acetonitrile and water. The samples were individually exposed to UV-LED 365 nm (M365L3, CW = 1.0 A (880 mW cm^{-2})) and Vis-LED 405 nm (M405L1,CW = 1.0 A, (1000 mW cm^{-2})) (Thorlabs Inc., Tampa, FL, USA). The power of the light source was controlled using a DC2200 (Thorlabs, Inc., USA). During exposure, UV-VIS spectra were acquired using a Cary 60 UV-Vis spectrophotometer (Agilent, Santa Clara, CA, USA).

2.7. Monitoring the photopolymerization processes by real-time FT-IR

A Thermo Scientific FT-IRi[10] NICOLET™ spectrometer with a horizontal adapter (Waltham, MA, USA) was used to monitor photopolymerization kinetics. The conversion of the monomer was calculated based on absorbance changes, specifically the decrease in the area of bonds corresponding to the presence of specific functional groups or bonds (involved in the light-induced polymerization process of the examined sample), using eqn (2):

$$\text{Conversion}\,[\%] = \left(1 - \frac{A_{after}}{A_{before}}\right) \times 100\% \quad (4)$$

where A_{after} is the area of the monitored band, and A_{before} is the starting value of this area of monitored band.

The light sources used were selected based on the absorption characteristics of the studied fluorophores and their potential use in 3D printing. The following light sources were used to study the photopolymerization process kinetics: 365 nm M365LP1 UV-LED (CW = 1.7 A (26.76 mW cm^{-2})) and 405 nm M405LP1 Vis-LED (CW = 1.4 A (29.73 mW cm^{-2})) (Thorlabs Inc., Tampa, FL, USA). A DC2200 controlled power supply (Thorlabs Inc., Tampa, FL, USA) was used to control the power of the light. The irradiation of the sample was started 10 s after the monitoring process began. The measured distance between the sample and the light source was 2.1 cm.

2.7.1. Free-radical photopolymerization processes with the use of multicomponent photoinitiating system and different water concentrations. The compositions for the study of the photopolymerization process kinetics using the real-time FT-IR method were prepared based on **PEGDA**. The oligomer-to-water ratios of the prepared resins ratio (8 : 2, 7 : 3, 6 : 4, and 5 : 5). The photoinitiating systems used in this case were based on 1.0 wt% of **IOD** and 0.1 wt% of each of the studied fluorophores. All compositions were examined under irradiation by the two light sources listed above (section 2.7). The experiments were carried out on a BaF_2 pallet with a 0.5 mm gouge to monitor samples of the same thickness. To ensure repeatability, all measurements were performed thrice, and the corresponding error bars were added when analyzing the results. The acrylate content was continuously monitored *via* FT-IR spectroscopy at approximately 6165 cm^{-1} for 600 s in air at 25 °C.

2.8. Monitoring of photopolymerization processes *via* photorheology measurements

Photo-rheological measurements were used to study the kinetics of photopolymerization processes through the change in viscosity of the system during irradiation using an MCR302e Rheometer with an adapter from Anton Paar Poland, which allows photo-rheological measurements. The experiments were conducted at a constant temperature of 25 °C maintained by a thermostat. A light source in the form of a 405 nm M405LP1 Vis-LED (CW = 1.4 A (13.37 mW cm^{-2})) was used for the measurements. To control the power of the light a DC2200 controlled power supply (Thorlabs Inc., Tampa, FL, USA) was used.

2.9. Kinetic studies of high-viscous compositions dedicated to extrusion-based 3D printing techniques

The compositions for kinetic studies of the photopolymerization process using the real-time FT-IR method were made based on **PEGDA** (70 wt%) in the role of the reactive part, and **PEG** (30 wt%) was used to increase the viscosity of the composition. The initiating system used in these compositions consisted of (1.0 wt%) of **IOD** and (0.1 wt%) of **TPA** and **CCA** fluorophores. The experiments were conducted in analogy to the previous ones under the irradiation of 405 nm M405LP1 Vis-LED (CW = 1.4 A (29.73 mW cm^{-2})) and on the BaF_2 pallet with a 0.5 mm gouge. The acrylate content was continuously monitored *via* FT-IR spectroscopy at approximately 6165 cm^{-1} for 600 s in air at 25 °C.

The compositions described above were studied using rheological and photorheological measurements. Tests were performed using an MCR302e Rheometer (Anton Paar, Graz, Austria). The experiments were conducted at 25 °C. Additionally, photo-rheological measurements included the use of an adapter from Anton Paar Poland that allowed photo-rheological measurements and a DC2200 controlled power supply (Thorlabs Inc., Tampa, FL, USA) to control the power of the light source (M405LP1 Vis-LED) (CW = 1400 A (13.37 mW cm^{-2})).

2.10. 3D printing experiments

The 3D printing experiments were conducted using a laser encoder printer (NEJE DK-8-KZ) equipped with a laser with a wavelength of 405 nm and an intensity of 1500 mW at a dis-

tance of 7 cm (spot diameter, ~75 μm). Stereolithography (SLA) printing was applied to low-viscosity compositions based on **PEGDA** (70 wt%) and water (30 wt%). The photoinitiating system consisted of 1.0 wt% **IOD** and 0.1 wt% **CCA** or **TPA** fluorophores. A light-sensitive resin with a thickness of 1 mm was placed on microscope glass.

For compositions showing higher viscosity, (70 wt% **PEGDA**, 30 wt% **PEG**, photoinitiating system: 1.0 wt% **IOD** and 0.1 wt% **CCA** or **TPA** fluorophore), a BioX™ printer (CELLINK, Goethenburg, Sweden) was applied. The studied compositions were transferred into a 3 ml plastic cartridge that was equipped with a corresponding tip-dispensing needle (with a diameter of 25 G = 0.5 mm). The extrusion parameters applied for the printing process were as follows: a pressure of 180–200 kPa and a speed of 20 mm s^{-1}. Photocrosslinking was performed using a built-in 405 nm emitting diode with an 9.88 mW cm^{--2} intensity at the sample.

To observe and analyze the final resolution of the obtained 3D printed objects a numerical optical microscope DSX-HRSU (Olympus, Tokyo, Japan) equipped with a DSX10-SXLOB3X objective lens with a magnification of 42–420× was utilized.

3. Results and discussion

3.1. UV-VIS absorption and photoluminescence characteristics

The greatest challenge currently posed to photosensitizers is to properly match their absorption spectra with the emission spectra of the LEDs used or the light source incorporated in the 3D printer, so that they can enhance the efficiency of the entire photopolymerization process. The absorption characteristics of the fluorophores were studied in acetonitrile and water (Fig. 3). The intention of applying the studied derivatives in compositions dedicated to the preparation of polymeric hydrogel materials, 3D printing from compositions containing the addition of water as a non-reactive agent, and the solvents were dictated by a more accurate reflection of the reaction environment. All studied compounds exhibited absorption ranging from 300 to 410 nm. All fluorophores showed a minor bathochromic shift (16–27 nm) upon switching from water to acetonitrile. However, for aqueous solutions, the UV-Vis spectra exhibited a hyperchromic effect owing to the increase in molar extinction coefficients by 2000 [dm^3 mol^{-1} cm^{-1}] with the spectra of the **ODPC** derivative, where the ε value exceeded 10 000 [dm^3 mol^{-1} cm^{-1}]. The fact that the spectra of all derivatives reach the visible range enables the use of light sources of higher wavelengths, making them safer and more suitable in the context of 3D printing applications. Owing to the broad UV-Vis absorption spectra of the studied derivatives, a wide range of UV and Visible light sources can be used to carry out the following measurements. The summarized spectroscopic properties of the investigated fluorophores in both solvents are shown in Table 1, emphasizing the molar extinction coefficients corresponding to the wavelength of the absorption maxima at 365 nm and 405 nm, taking into account further analyses using light sources that emit light at these wavelengths.

3.2. Electrochemical determination of oxidation and reduction potential

Cyclic voltammetry studies of the investigated fluorophores were conducted to determine their photooxidation and photoreduction potentials, as well as the following calculation describing the probability of an effective electron transfer process based on the probability and efficiency of light-initiated polymerization. Examples of cyclic voltammetry curves obtained for **CCA** derivatives are shown in Fig. 4a and c,

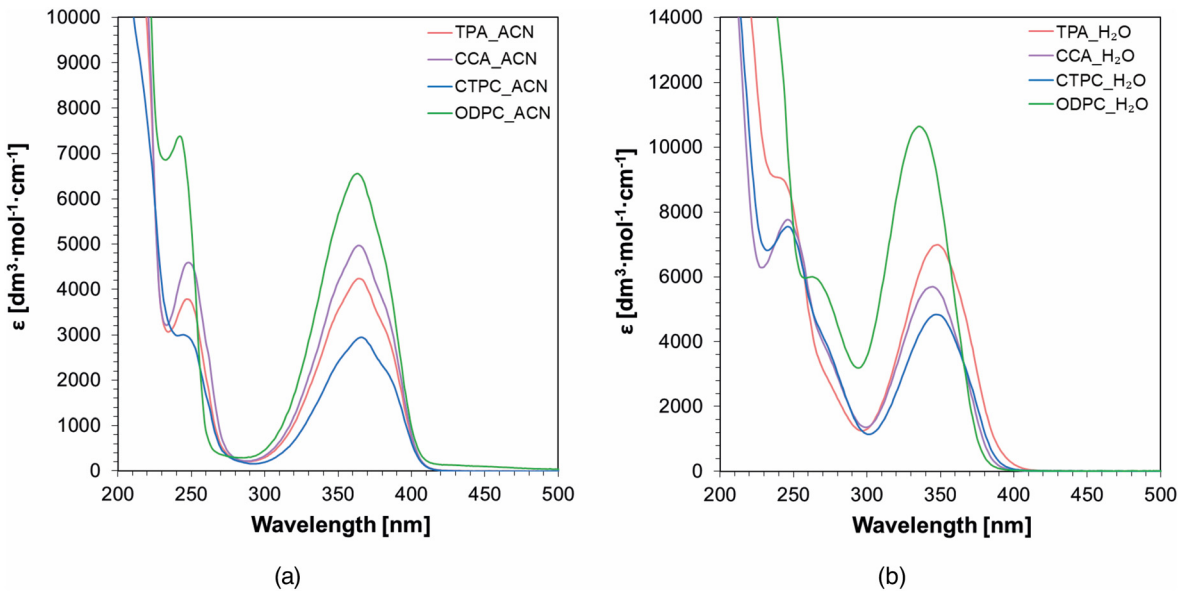

Fig. 3 UV-Vis absorption spectra of studied fluorophores in (a) acetonitrile and (b) distilled water.

Table 1 Spectral characteristics of newly synthesized fluorophores studied in acetonitrile and distilled water

	Acetonitrile				Water			
Acronym	λ_{max} [nm]	ε_{max} [dm^3 mol^{-1} cm^{-1}]	ε_{365} [dm^3 mol^{-1} cm^{-1}]	ε_{405} [dm^3 mol^{-1} cm^{-1}]	λ_{max} [nm]	ε_{max} [dm^3 mol^{-1} cm^{-1}]	ε_{365} [dm^3 mol^{-1} cm^{-1}]	ε_{405} [dm^3 mol^{-1} cm^{-1}]
TPA	364	4240	4237	296	348	6986	5134	112
CCA	364	4973	4967	394	345	5699	3485	28
CTPC	366	2948	2942	266	347	4839	3439	35
ODPC	363	6558	6515	450	336	10 634	3592	24

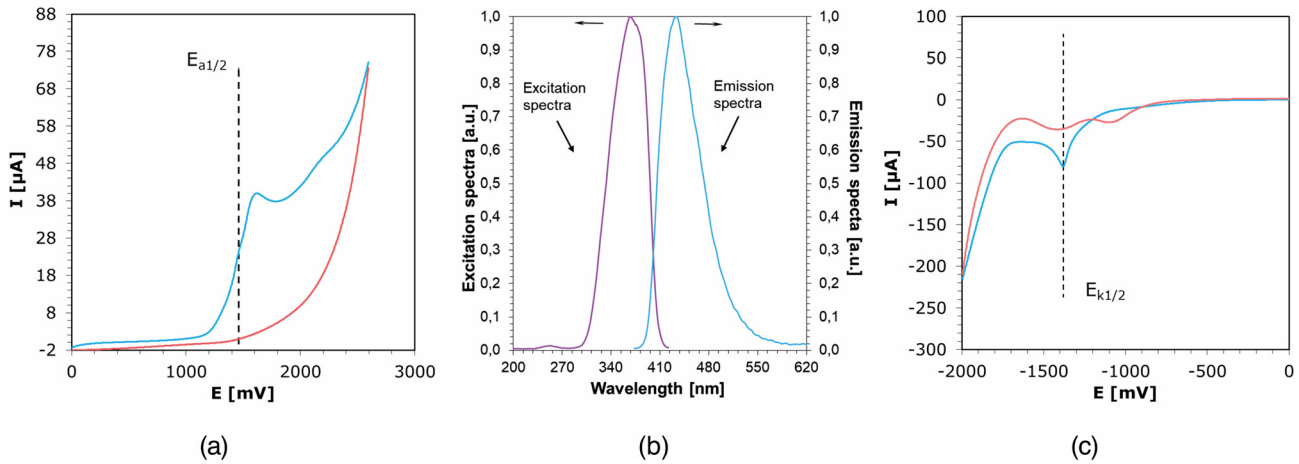

Fig. 4 (a) Cyclic voltammetry for oxidation process (CVox, *vs.* Ag/AgCl) experiments in ACN (containing 0.1 M tetrabutylammonium hexafluorophosphate) for **CCA**; (b) excitation and emission spectra for the determination of the excited singlet state energy for **CCA** for the solution in acetonitrile; (c) cyclic voltammetry for reduction process (CVred, potential *vs.* Ag/AgCl) experiments in ACN (containing 0.1 M tetrabutylammonium hexafluorophosphate) for **CCA**.

along with the excitation and emission spectra determined for solutions of these compounds in acetonitrile (Fig. 4b). Complementary cyclic voltammetry curves for the rest of the studied compounds are shown in Fig. S22–S27 in the ESI.†

Citric-acid-derived fluorophores have been proposed as photosensitizers in photoinitiating systems based on electron transfer *via* photo-oxidation mechanisms. In this case, the studied compounds acted as electron donors and were subjected to oxidation during the process. In the described electron transfer process, iodonium salt, on the other hand, undergoes reduction, which makes it an electron acceptor during the process. Electrochemical assessments and subsequent thermodynamic calculations were performed to confirm the validity of the designed photoinitiating systems. A summary of the results is presented in Table 2.

To determine the Gibbs free energy (ΔG), the conventional Rhem–Weller equation was used, which is based on the oxidation potentials of the fluorophores. The negative values of

Table 2 Electrochemical and thermodynamically properties of citric acid derived fluorophores in terms of their use in photo-oxidation mechanism in light induces electron transfer process

	Singlet state energy	Electrochemically determined potentials		Photo-oxidation	Photo-reduction
Acronym	E_{00} [eV]	E_{ox} [mV]	E_{red} [mV]	ΔG_{IOD} [a] [eV]	ΔG_{MDEA} [a] [eV]
CCA	3.22	1484	−700	−1.10	−1.66
TPA	3.24	1696	−825	−0.90	−1.55
CTPC	3.21	1621	−532	−0.95	−1.81
ODPC	3.24	1383	−688	−1.22	−1.69

[a] **Ca**lculated from the classical Rehm–Weller equation: $\Delta G_{et} = F[E_{ox}(D/D^{\bullet+}) - E_{red}(A^{\bullet-}/A)] - E_{00} - \left(\frac{N_A e^2}{4\pi\varepsilon_0\varepsilon_r a}\right)$. $E_{ox}(D/D^{\bullet+})$ – electron donor's electrochemically determined oxidation potential (0.864 V for MDEA *vs.* Ag/AgCl).[75] $E_{red}(A^{\bullet-}/A)$ – electron acceptor's electrochemically determined reduction potential (−0.64 V for **IOD** *vs.* Ag/AgCl).[76,77] E_{00} – sensitizer's singlet state energy determined based on emission and excitation spectra.

ΔG obtained for the photoinitiating systems based on the studied derivatives and iodonium salt indicate that the developed systems can work effectively in the case of initiating the light-induced polymerization process, as they are thermodynamically acceptable. The most outstanding and lowest values were obtained for **CCA** and **ODPC** derivatives, namely for derivatives with the simplest structure, which, compared to the others, have only one carboxyl group in their structure. However, in comparison, they differ in the number of carbons in the second aliphatic ring and built-in electrophiles, which are sulfur and oxygen, respectively. The lower ΔG value for **CCA** is perfectly understandable and justified by the presence of sulfur in the structure, which has a higher electron-donor potential than the oxygen embedded in the **CCA** structure.

The studied derivatives were also tested electrochemically for type II photoinitiating systems, where they act as electron acceptors, because this type of photoinitiating system corresponds to electron transfer between electron acceptors and another molecule, namely the co-initiator. A two-component system based on MDEA and the investigated fluorophores can effectively work in this type of initiating system, where the citric acid derivatives act as electron acceptors and are reduced during the process, while MDEA acts as a co-initiator, being an electron donor that undergoes oxidation due to electron transfer. The results of the electrochemical analyses performed to assess the electron transfer abilities and thermodynamic properties of the studied compounds are summarized in Table 2.

The Gibbs free energy (ΔG) was determined for type II photoinitiating systems. Owing to the negative values of ΔG obtained after appropriate calculations, it was possible to confirm the thermodynamic acceptability of the studied electron transfer process. The lowest ΔG values were obtained for ODCP, **CTPC**, and **TPA** derivatives (in ascending order). In the case of the **ODPC** derivative, we deal with the least complicated structure, whereas in comparison with the other two, it has more carbons in the second aliphatic ring, and the embedded atoms are nitrogen and oxygen, not nitrogen and sulfur, as in the other cases. In the case of **CTPC** and **TPA** derivatives, compared to the one for which the lowest value was obtained, they stand out because they have two electron acceptor carboxyl groups. The presence of such groups can negatively affect the electrochemical properties, which may explain why they have higher ΔG values than other fluorophores in the case of an oxidative cycle. In addition, the complexity of the structure may negatively affect the obtained values.

In summary of the results obtained and their interpretations, it is possible to conclude that the studied fluorophores are preliminary suitable for the role of iodonium salt (**IOD**) photosensitizers (which are the subject of the following research) as well as type II initiating systems.

3.3. Determination of average fluorescence lifetimes

A time-correlated single-photon counting system (TCSPC) was used to investigate the average fluorescence lifetimes of the citric-acid-derived fluorophores. The average lifetimes are not only a complementary element for the spectroscopic characterization of the compounds studied, but in combination with appropriate studies, such as fluorescence quenching, they allow the determination of the parameters of the electron transfer process and the identification of its mechanism. The curves of the decay, reference (Ludox), and fit for the **CCA** derivative are shown in Fig. 5a and b, alongside the residuals obtained for the calculated fit. The remaining curves are shown in Fig. S34–S39 in the ESI.† The results obtained for the samples in distilled water and acetonitrile are presented in Table 3 together with the wavelength corresponding to the maximum emission.

The obtained values of the average time for which the investigated fluorophores ended in the excited state before returning to the ground state varied between 8 and 13 ns. The highest values were obtained for the **ODPC** fluorophore, which is the simplest structure, and the lowest value for the most complex of the studied derivatives, **CTPC**. For the two remaining compounds that were most similar in structure, the one designated as **TPA** showed higher average fluorescence lifetimes. Thus, this correlation can be attributed to the presence of an additional carboxyl group in the aforementioned molecule compared with the less complex analog **CCA**. All compounds showed higher values when acetonitrile was used as the solvent than when acetonitrile was used in distilled water. The accuracy of the measurements was validated by the low-deviation values in the residual curves. Additionally, it is important to note that the chi-square test values used to calculate the corresponding fits in all cases varied from 1.00 to 1.20, suggesting a statistically acceptable correlation.

Spectrofluorimetric analysis of the emission spectra of the studied chromophores was performed to evaluate and compare the emission intensities of the studied chromophores and to correlate them with other spectroscopic properties. The emission spectra for all compounds in acetonitrile and distilled water are shown in Fig. 6a and b. The normalized excitation and emission spectra for each chromophore are shown in Fig. S15–S21 in the ESI.† The λ_{max} of the emission spectra, as well as the corresponding intensities, are shown in Table 4.

The chromophores with the acronyms **CCA** and **TPA** achieved the lowest emission intensities of over 10^5 for both solutions. However, the additional carboxyl group present in **TPA** appears to have slightly increased the intensity. Further expansion of the basic structure allows the emission intensity values to reach almost four times higher. However, the highest values in both cases were achieved for the compound with the acronym **ODPC**, which is the only compound with oxygen in its structure instead of sulfur. Analogous to the earlier studies of absorption properties, in the case of emission, we observed a shift of the spectral maximum towards longer wavelengths for solutions in acetonitrile.

3.4. Fluorescence quenching and mechanism of electron transfer from the excited state

Fluorescence quenching measurements complementary to average fluorescence lifetime studies were carried out to define the mechanism of electron transfer from the excited state. The

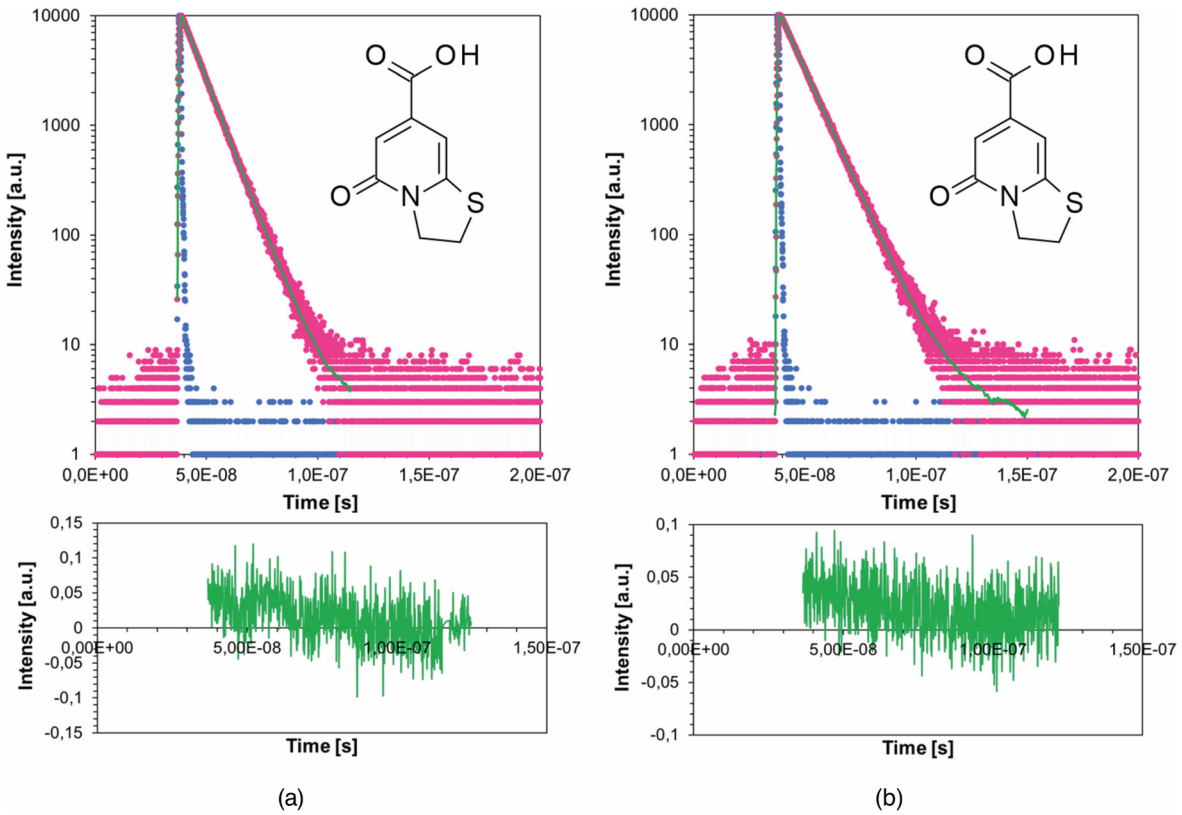

Fig. 5 Fluorescence lifetimes measurements conducted for **CCA** fluorophore in (a) distilled water and (b) acetonitrile showing sample's decay, reference and model fit used to calculate the precise fluorescence lifetimes along with model residuals obtained for each of the curves respectively.

Table 3 Summary of the obtained average fluorescence lifetimes for the studied fluorophores in distilled water and acetonitrile as solvents 3 together with chi-squared test values of the corresponding fit curves used for average fluorescence lifetimes calculations

Acronym	$T_{(S1)}$ ACN [ns]	χ^2 ACN	$T_{(S1)}$ H_2O [ns]	χ^2 H_2O
CCA	9.63	1.15	8.26	1.11
TPA	10.04	1.17	9.94	1.08
CTCP	9.44	1.08	7.45	1.16
ODPC	10.88	1.12	12.57	1.06

changes in the emission spectra depending on the concentration of the fluorescence quenching agent in the form of the diphenyliodonium salt (**IOD**) for the **CCA** fluorophore, along with the Stern–Volmer plot for all compounds, are shown in Fig. 7a and b. The remaining results for all fluorophores are shown in Fig. S31–S33 in the ESI.†

For all derivatives, a linear relationship was apparent between the increasing fluorescence quencher concentration and the ratio of the initial intensity to the intensity obtained with subsequent **IOD** addition. The Stern–Volmer plots for each of the fluorophore solutions were characterized by a correlation coefficient of $R^2 > 0.99$, so that the results can be described as statistically acceptable and valid. Therefore, it was possible to calculate the quantum yields of electron transfer from the excited state ($\Phi_{et(S1)}$) and electron transfer constant (k_q) for all fluorophores. The calculation results are presented in Table 5. The obtained quantum yields differed only slightly; however, it is possible to assume that the **CCA** fluorophore participated most effectively in the studied electron transfer process. The electron transfer constants indicate that, in all the cases studied, static quenching takes place at $k_q < 2 \times 10^{10}$, which means that quenching occurs because of the formation of a complex between the fluorophore and the quenching molecule.

3.5. Steady state photolysis of citric acid derived fluorophores

Photostability measurements were carried out to determine the possibility of using the designated fluorophores as photosensitizers of diphenyliodonium salt in free-radical photopolymerization processes. Measurements carried out for all fluorophore solutions using 405 nm VIS-LED are shown in Fig. 8a and those containing an additionally 1.86×10^{-4} mol dm^{-3} of **IOD**. The results of the complementary photostability studies using LED at 365 nm and for aqueous solutions of the studied chromophores are shown in Fig. S28–S30 in the ESI.†

The ability of a specific compound is dictated by the presence of electron-donor groups in the structure of the compounds investigated, where in the case presented within the framework of this paper we are dealing with electron-donors in the form of oxygen in hydroxyl and carbonyl groups or sulfur and nitrogen in heterocyclic systems. However, the key role on

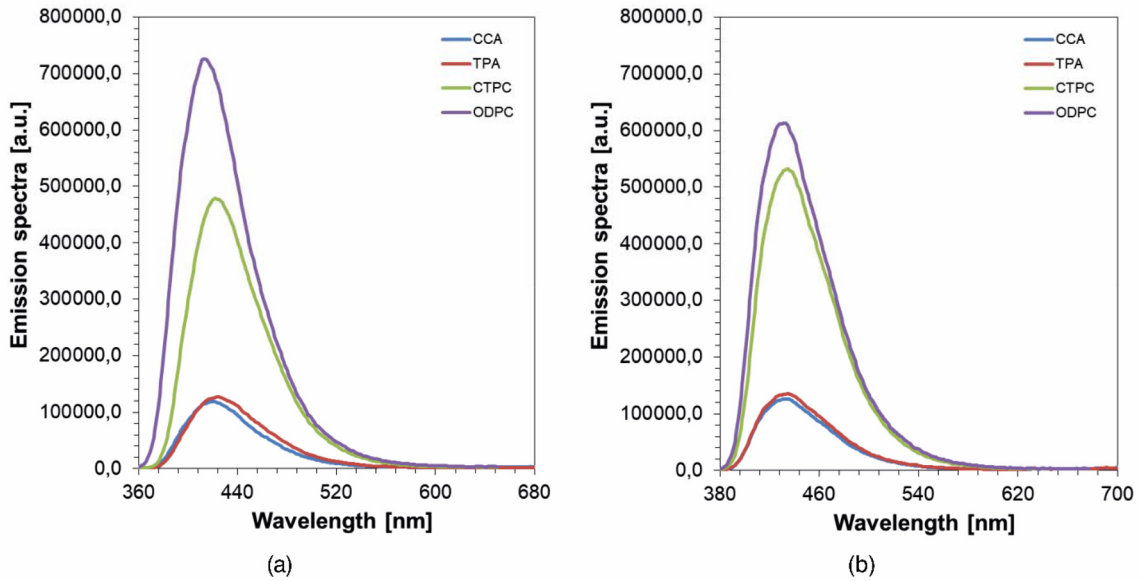

Fig. 6 Emission spectra of all the studied chromophores in (a) distilled water and (b) acetonitrile showing fluorescence intensity of the studied compounds.

Table 4 Summary of the maximum of emission for all of the chromophores in acetonitrile and distilled water together with the corresponding intensities

Acronym	λ_{max} ACN [nm]	I_{max} ACN	λ_{max} H_2O [nm]	I_{max} H_2O
CCA	433	1.27×10^5	420	1.19×10^5
TPA	434	1.35×10^5	423	1.27×10^5
CTCP	434	5.32×10^5	422	4.79×10^5
ODPC	432	6.13×10^5	412	7.26×10^5

the susceptibility to photodecomposition during irradiation with a light source emitting electromagnetic radiation of a particular wavelength is played by the value of the molar extinction coefficient obtained for that particular wavelength. Photostability studies showed that all the studied derivatives underwent photodegradation when exposed to irradiation at 365 nm. This is mostly due to the fact that the maximum absorption bands for all of the studied fluorophores in this case correspond to the wavelengths of the light source, so the process can occur more effectively. In the case of irradiation

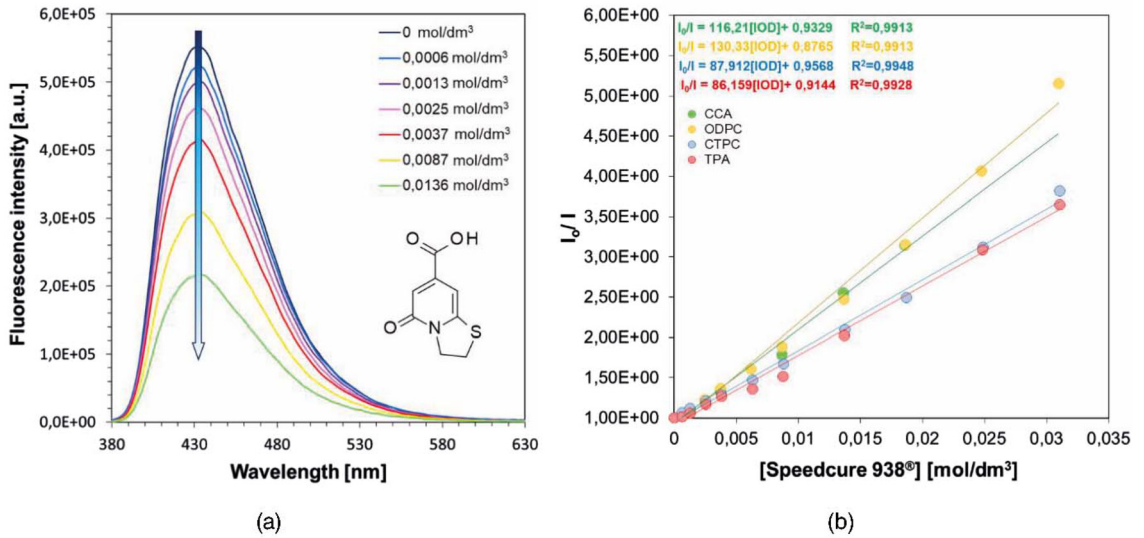

Fig. 7 Fluorescence quenching measurements shown by (a) change in intensity of emission spectrum for **CCA** derivative under increasing concentration of quenching agent – **IOD**. (b) Stern–Volmer plot showing dependence of normalized maximum emission intensity on concentration of quenching agent.

Table 5 Summary of the obtained parameters form Stern–Volmer equation (K_{SV}), quantum yields of electron transfer from the excited state ($\Phi_{et(S1)}$), average fluorescence lifetimes ($\tau_{(S1)}$) and electron transfer constant (k_q) for the studied fluorophores in acetonitrile

Acronym	K_{SV} [M^{-1}]	$\Phi_{et(S1)}$	$\tau_{(S1)}$ [ns]	k_q [M^{-1} s^{-1}]
CCA	116.21	0.71	9.63	1.21×10^{10}
TPA	85.16	0.64	10.04	8.48×10^{9}
CTPC	87.91	0.65	9.44	9.31×10^{9}
ODPC	107.41	0.69	10.88	9.87×10^{9}

with lower energy (405 nm), the changes in absorption spectra are minimal in most cases; only the **ODPC** fluorophore shows significant changes in acetonitrile, although in this case the spectra are shifted towards higher wavelengths compared to other compounds. Overall, these results indicate that the studied fluorophores have the potential to be applied in photoinitiating systems based on **IOD** for free-radical photopolymerization.

3.6. Investigation of photopolymerization processes by real-time FT-IR

Taking in account the absorption spectra of studied derivatives and the potential 3D printing applications the photopolymerization processes were carried out using 365 nm UV-LED (CW = 1.7 A (26.76 mW cm^{-2})) and 405 nm VIS-LED (CW = 1.4 A (29.73 mW cm^{-2})). An additional objective of FT-IR analysis was to determine the effect of the water content of the composition on the kinetics of the photopolymerization process and the possibility of using the developed systems to obtain hydrogel materials.

3.6.1. Free-radical photopolymerization processes with the use of multicomponent photoinitiating system and different water concentrations. The applicability of the citric acid fluorophores as photosensitizers of **IOD** was first tested using hydrogel compositions based on the **PEGDA** oligomer with a number-average molar mass of M_n = 700 g mol^{-1} and water as the non-reactive component in appropriate weight ratios. The photoinitiating system tested in these cases contained 1.0 wt% **IOD**, 0.1 wt% photosensitizer, each of the fluorophores tested, and the matrix content was an oligomer (80 wt%, 70 wt%, 60 wt%, 50 wt%) with a corresponding water content (20 wt%, 30 wt%, 40 wt%, 50 wt%). The tested reference compositions differed only in the photoinitiating system, which contained only 1.0 wt% **IOD**. The results, specifically the final conversions obtained for all the compositions tested, are shown in Fig. 9a–d. Kinetic profiles for the respective compositions are presented in the ESI in Fig. S40–S47.†

The aim of this part of the research was mainly to determine the suitability of the studied compounds as photosensitizers of **IOD** and to select systems that would show the best efficiency of the initiation process, leading to final conversion values that allow the use of the developed compositions to obtain hydrogel materials by 3D printing methods. The secondary objective was to determine the influence of the water content as a non-reactive component on the course of the process, particularly on the final conversion values of the double bonds present in the acrylate oligomer.

In accordance with previously obtained results of analyses of the potential efficiency of the studied photosensitizers, such as cyclic voltammetry and studies of the electron transfer mechanism based on fluorescence quenching, as well as measurements of average fluorescence lifetimes, the **CCA** fluorophore showed the highest efficiency in the case of catalyzing the initiation of radical photopolymerization according to the radical mechanism. Compositions containing the initiating systems based on **CCA** and **TPA** fluorophores showed the

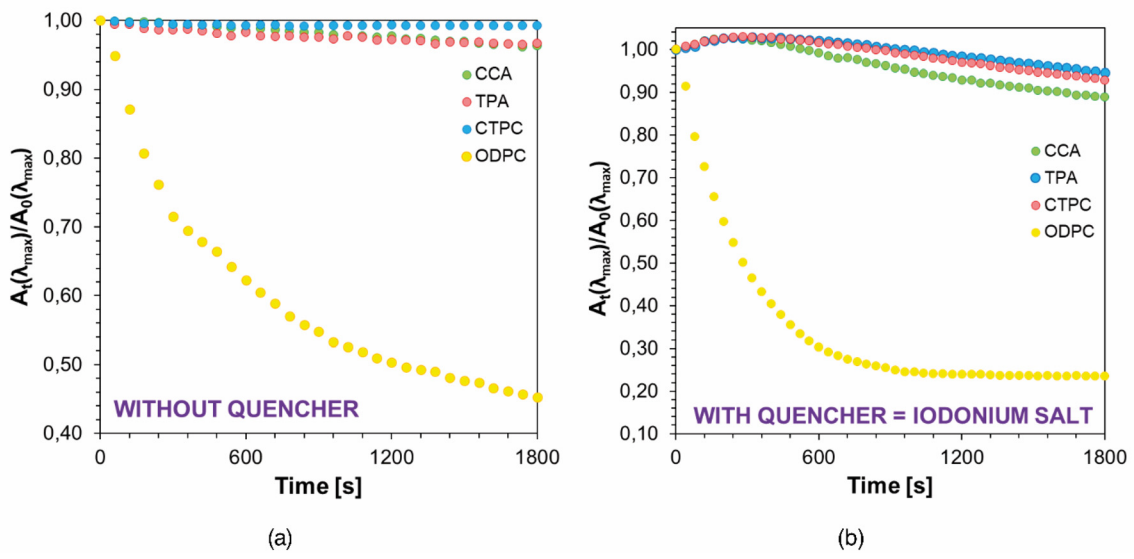

Fig. 8 Photo-decomposition of (a) all of the chromophores in acetonitrile and (b) the same solutions with the addition of **IOD** (1.86×10^{-4} mol dm^{-3}) carried out for 30 minutes during irradiation with 405 nm UV-LED at 1.0 A (1000 mW cm^{-2}) shown as the corresponding absorbance correlation at the absorbance maximum (λ_{max}).

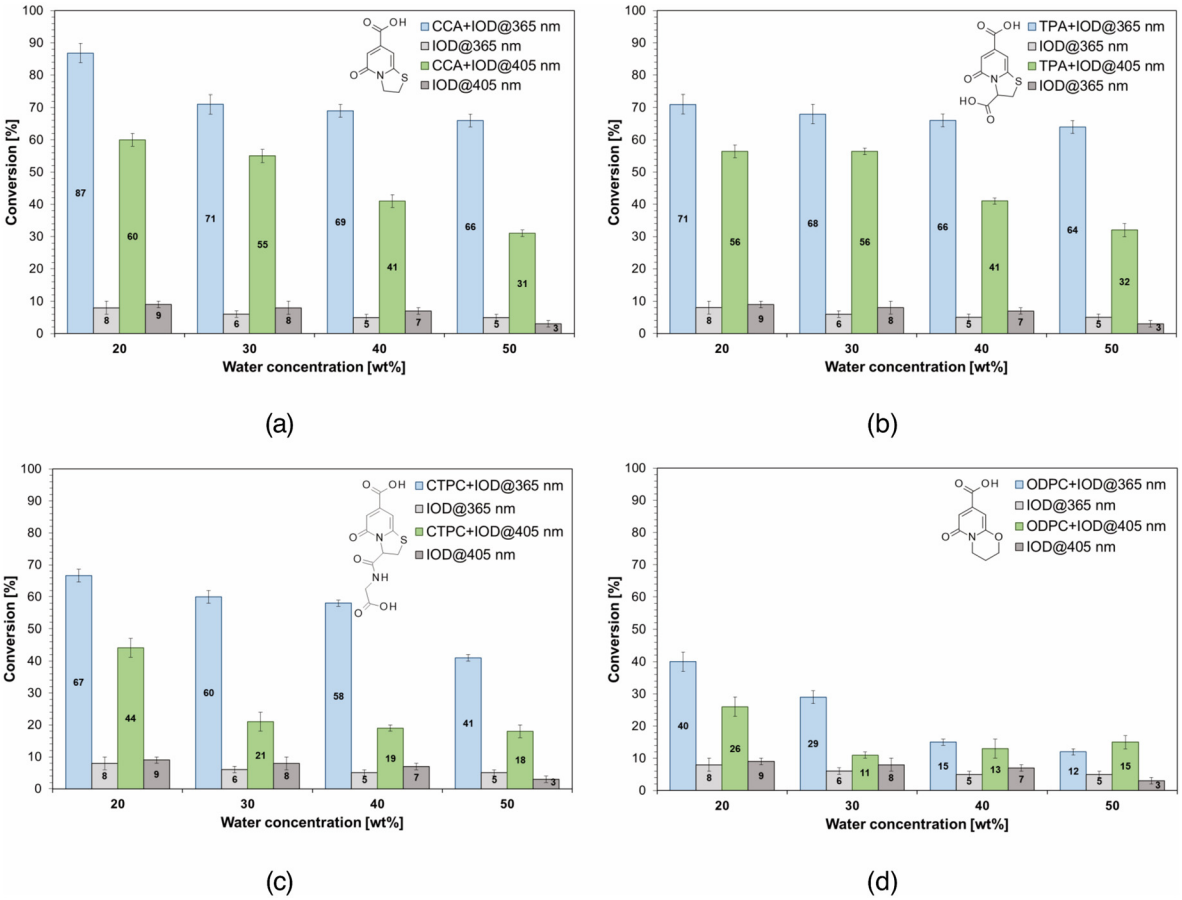

Fig. 9 Comparison of maximum conversions of acrylate oligomer (**PEGDA** M_n = 700 g mol^{-1}) during photopolymerization process occurring according to radical mechanism obtained using various initiating systems using respectively 0.1 wt% of the photosensitizers, respectively, (a) **CCA**, (b) **TPA**, (c) **CTPC** and (d) **ODPC** and 1.0 wt% photoinitiator – **IOD** are displayed on the data bars. The results were grouped according to the water content in the formulation. The results were obtained during irradiation with a light-emitting diode with a wavelength of 365 nm (CW = 1.7 A (26.76 mW cm^{-2})) and 405 nm (CW = 1.4 A (29.73 mW cm^{-2})). As references, photopolymerization processes involving a citric acid chromophore-free inking system are shown (grey). The results were grouped according to the quantity of water in the light-curable composition and shown together with the corresponding error bars for the three repeated measurements.

highest final conversion values, as indicated by the presence of sulfur in the structures of both photosensitizers. The lower values obtained for **CTPC** may be related to the complexity of this structure, specifically, the group attached to the carbon in the third position. As can be seen, the simplest chromophore shows the highest efficiency, the substitution of the carboxyl group causes a slight decrease in the efficiency of the initiation process. In the case of a larger substituent containing atoms and groups of different natures, the potential is significantly reduced, possibly indicating intramolecular processes that may lead to a decrease in the efficiency of catalysis of the initiation process. In the case of the **ODPC** chromophore, the lowest values were obtained, although this was not indicated by previous analyses, in which it showed the best properties, apart from **CCA**. However, it could already be concluded that it may have the lowest efficiency owing to the presence of oxygen in the structure, which indicates a lower probability of electron transfer than that in the case of sulfur, which is incorporated into the other chromophores. However, based on other results in which this chromophore showed very good spectroscopic and electrochemical properties, it would indicate a much higher efficiency. The conversion values were also higher when light of shorter wavelengths was used, which is related to the fact that all the compounds studied exhibit significantly higher molar extinction coefficient values at this wavelength.

A secondary aim of these analyses was to determine the influence of the water content of the composition on the final conversion values, and possibly the course of the photopolymerization process. Regarding the course of the process, specifically the kinetic profiles included in the ESI in Fig. S40–47,† no conclusive differences were observed. However, the differences in the final conversion values were significant. In the case of both diodes and all initiating systems, the final conversion values decreased with increasing water content in the composition. This relationship may be related to the lower content of the reactive component, the **PEGDA** oligomer, which affected the lower intensity of the observed band associated with the lower content of reactive double bonds, the clea-

vage of which was monitored. Increasing the dilution of the composition negatively affects the process, leading to lower conversion values. In some cases, this dilution is preferred because it eliminates excessive crosslinking of the composition, which can cause problems in the case of 3D printing using an acrylate oligomer with significant reactivity. On the basis of the results obtained, it was determined that a water content of 30% allowed the composition to be crosslinked effectively without negatively affecting the final conversion values.

3.7. Monitoring of photopolymerization processes *via* photorheology measurements

The aim of the photorheology studies was to validate the results obtained from the preceding analyses of the photopolymerization process using the real-time FT-IR method and to determine parameters such as polymerization shrinkage and gel time (τ_{gel}), which are crucial for the use of the investigated compositions in 3D printing processes. The results of polymerization shrinkage for all of the compositions based on the initiating system are presented in Fig. 10a, and the corresponding changes in the storage modulus for the compositions based on **CCA** chromophore in the role of photosensitizer are shown in Fig. 10b. The gel times for the respective initiating systems per composition are shown in Table 6. Complementary results obtained for other photoinitiating systems are shown in Fig. S48–S50 in the ESI.†

The photorheology measurements enabled the determination of polymerization shrinkage, which is one of the key parameters in the application of the compositions studied in 3D printing. The excessive shrinkage percentage, that is, the difference in the thickness of the composition before and during the photopolymerization process, affects the accuracy of the structure obtained as a result of 3D printing and its compliance with the initial digital project. For the studied samples, the polymerization shrinkage increased as a result of increasing dilution of the composition. The latter is because photopolymerization reactions are highly exothermic processes, and the irradiation itself also increases the temperature of the sample, which makes it possible for the diluent in the form of water to partially evaporate, resulting in a change in the volume of the sample tested during measurements. The percentage of final shrinkage was not significant (0.3% for a water content of 50 wt%); however, for a potential application

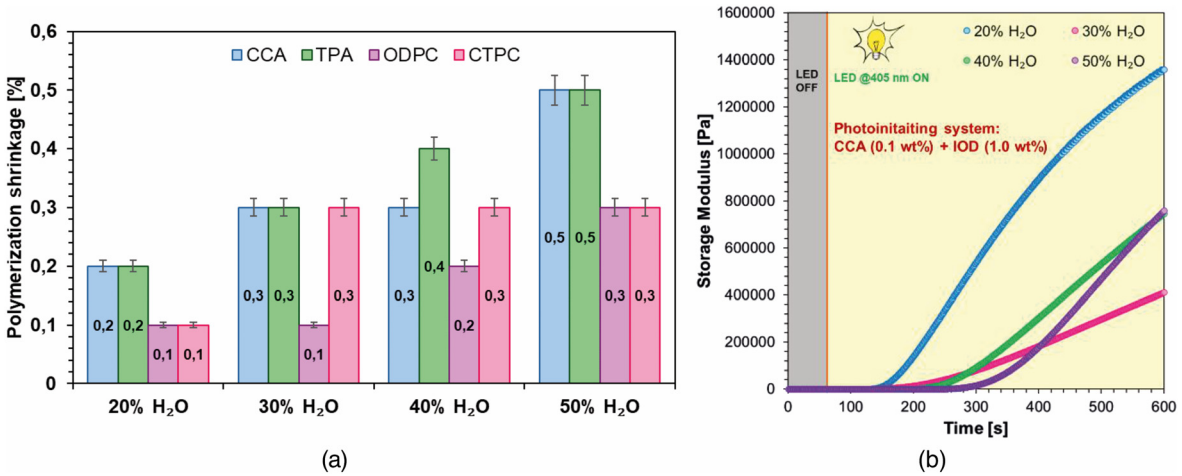

Fig. 10 (a) Polymerization shrinkage final values for compositions containing all of the chromophores (0.1 wt%) and **IOD** (1.0 wt%) with **PEGDA** oligomer (80 wt%, 70 wt%, 60 wt%, 50 wt%) and water (20 wt%, 30 wt%, 40 wt%, 50 wt%) monitored for 600 s, under irradiation with a light source of 405 nm at an intensity of 1.4 A (13.37 mW cm^{-2}). The results were grouped according to the quantity of water in the light-curable composition. (b) Changes in the storage modulus (G') during photopolymerization depicted for compositions with different water concentrations and containing a photoinitiating system with **CCA** (0.1 wt%) and **IOD** (1.0 wt%).

Table 6 Summary of gel times (τ_{gel}) obtained for all initiating systems containing 0.1 wt% fluorophore, 1.0 wt% **IOD** and respective amounts of **PEGDA** oligomer and non-reactive component in the form of distilled water, respectively

	τ_{gel} [s]			
Photoinitiating system	80 wt% **PEGDA** 20 wt% H_2O	70 wt% **PEGDA** 30 wt% H_2O	60 wt% **PEGDA** 40 wt% H_2O	50 wt% **PEGDA** 50 wt% H_2O
0.1 wt% **CCA** + 1.0 wt% **IOD**	108	112	169	203
0.1 wt% **TPA** + 1.0 wt% **IOD**	88	93	105	108
0.1 wt% **CTPC** + 1.0 wt% **IOD**	104	146	225	284
0.1 wt% **ODPC** + 1.0 wt% **IOD**	146	155	196	357

in 3D printing, it was necessary to select a composition with the lowest possible polymerization shrinkage using the highest possible diluent content. In the case of a composition containing 30 wt% distilled water and 70 wt% **PEGDA** oligomer, the polymerization shrinkage remains at the same level as that of the least diluted sample, increasing only towards the end of the process. However, by using a shorter exposure time in the printing process, a lower shrinkage value can be maintained during the 3D printing process.

It is also important to select a composition with process initiation efficiency that would allow rapid production of polymeric materials by 3D printing methods. The gel point and the corresponding gel time corresponded to the point at which the rheological properties of the sample changed; thus, polymerization and crosslinking of the tested composition occurred. For a composition that was preselected for printing and contained 30 wt% water, the lowest gel times corresponded to compositions with a photoinitiating system containing the fluorophores **TPA** and **ODPC** as photosensitizers. However, considering the previously obtained results from real-time FT-IR measurements and the effectiveness of the system in terms of the final conversion values obtained for the double bonds present in the acrylate oligomer, the initiating system containing the fluorophore **ODPC** did not allow the formation of suitable values. Therefore, compositions based on an initiating system containing 0.1 wt% of the photosensitizer **CCA** or **TPA** and 1.0 wt% **IOD**, respectively, as well as the oligomer PEDGA 70 wt% and distilled water 30 wt% were selected for the 3D printing process. The choice of composition was dictated by both photorheology and real-time FT-IR results included in Fig. 11. Although the induction time in the case of photorheology studies was considerably higher than for FT-IR analyses, the main purpose of the studies presented in this section was to determine polymerisation shrinkage. In addition, the induction times are higher in this case due to the light intensity on the sample being less than twice as high as for FT-IR studies due to the specifics of the measurement system.

3.8. Kinetic studies of high-viscous compositions dedicated to extrusion-based 3D bioprinting techniques

Having in mind the possible application of the investigated initiation systems in 3D bioprinting based on pressure extrusion of photocurable materials, *i.e.* in DIW (direct ink writing) technology, the compositions were modified in such a way as to meet the criteria for bioinks used in this 3D printing technology. In order to achieve this, **PEG** with an average molar mass of M_n = 2000 g mol^{-1} in the same amount as distilled water *i.e.* 30 wt%, was applied instead of distilled water as a diluent and 80 wt% of **PEGDA** oligomer with an average molar mass of M_n = 700 g mol^{-1}, while the initiator **IOD** (1.0 wt%) and the fluorophore **CCA** or **TPA** (0.1 wt%) served as the initiating system. In the context of applying the proposed compositions to DIW 3D printing processes, it is crucial to determine the changes in rheological properties during sample exposure to light. Classic rheological studies were carried out to examine the viscosity of the compositions compared to commercially used bioinks to determine the usefulness of extrusion, where viscosity is of key importance in determining the printing parameters. A graph showing the time dependence of the storage modulus, loss modulus and normal force for the composition containing 30 wt% **PEG** and 70 wt% photoinitiating system with 0.1 wt% **CCA** and 1.0 wt% **IOD** is shown in Fig. 12a and the viscosity obtained for each composition tested and commercial CELLINK START are shown in Fig. 12b.

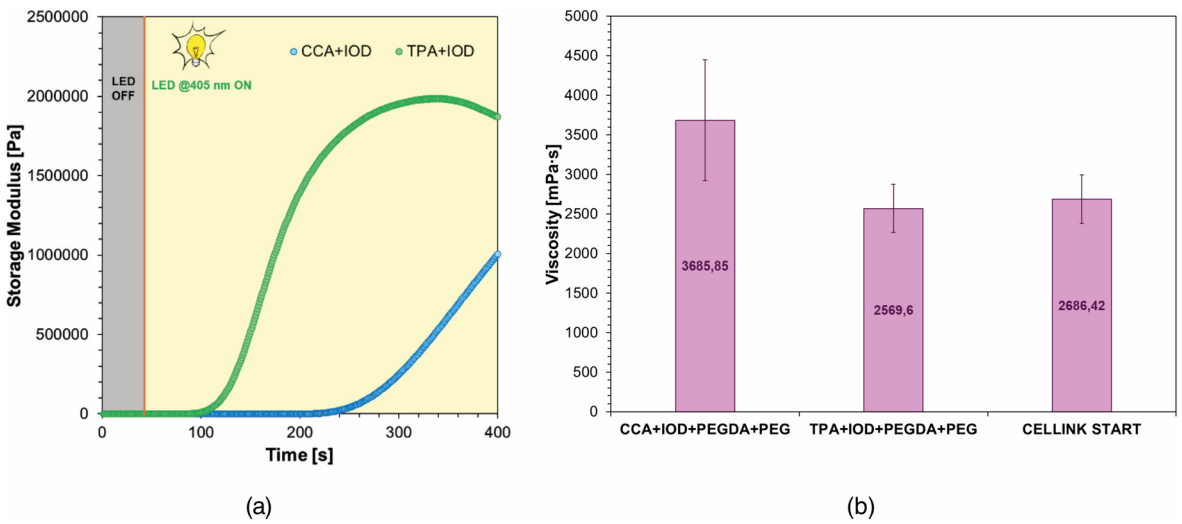

Fig. 11 (a) Kinetic curves obtained from rheological measurements for the compositions containing **PEGDA** (70 wt%) in the role of the reactive part and **PEG** (30 wt%) as a non-reactive part with a corresponding initiating system consisting of (1.0 wt%) **IOD** and (0.1 wt%) **CCA** and **TPA** fluorophore, respectively. The samples were monitored for 600 s, under irradiation with a light source of 405 nm at an intensity of 1.4 A (13.37 mW cm^{-2}). (b) Viscosity of the composition containing **CCA** or **TPA** (0.1 wt%) and **IOD** (1.0 wt%) with **PEGDA** oligomer (70 wt%) and **PEG** (30 wt%) along with the obtained final viscosity value and the value obtained for the commercially used bioink CELLINK START.

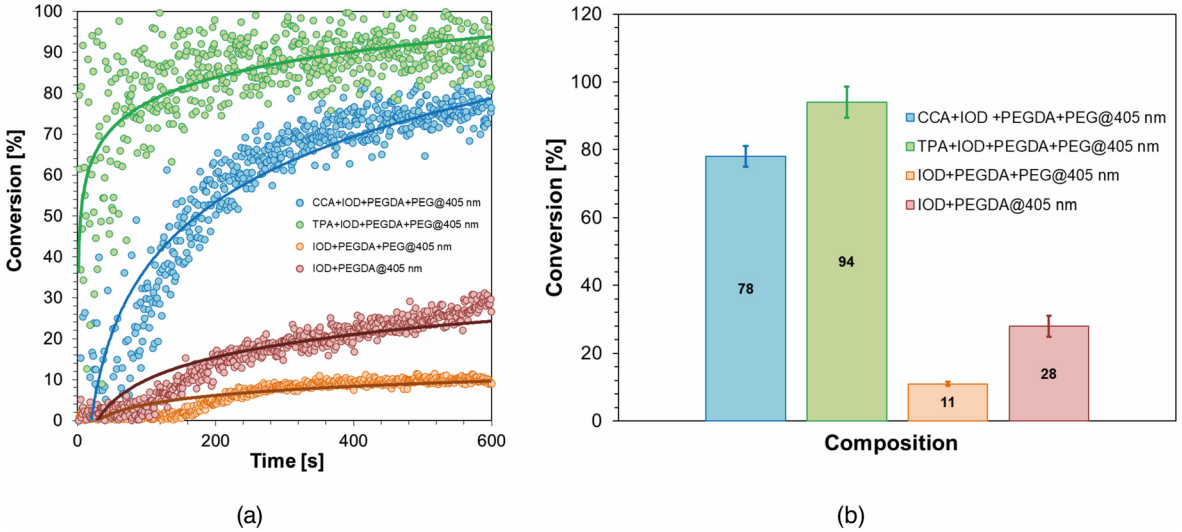

Fig. 12 (a) Kinetic profiles obtained for the monitored band at wavenumber 6165 cm^{-1} for compositions containing, respectively, **CCA** or **TPA** (0.1 wt%) and **IOD** (1.0 wt%) with **PEGDA** oligomer (70 wt%) and **PEG** (30 wt%) as the non-reactive component. (b) Comparison of final conversions of acrylate oligomer (**PEGDA** M_n = 700 g mol^{-1}) during photopolymerization process occurring according to radical mechanism. The results were obtained during irradiation with a light-emitting diode with a wavelength of 405 nm (CW = 1.4 A (29.73 mW cm^{-2})).

From the photo-rheological studies carried out, it was possible to determine the gel time for the application of 405 nm light of an appropriate intensity to the sample (13.37 mW cm^{-2}), which is a key parameter in terms of the use of the compositions studied in 3D printing, as it allows us to determine the exposure time of the structure obtained by extrusion of the high-viscosity bioink for its cross-linking. In the case of a composition containing an initiating system based on the fluorophore **TPA** as a photosensitizer, it was possible to significantly reduce the time needed to reach the gel point, so that the exposure time of the obtained structure could be shortened compared to the other compositions. In this case, the gel point was determined as the point of inflection of the loss modulus and storage modulus, and not as the point of intersection, as these moduli are far apart because of the high viscosity of the material.

To determine the usefulness of the compositions tested for 3D printing, real time-FT-IR analyses were also carried out to thoroughly investigate the possibility of post-curing of the extruded structure and thus confirm the results obtained by photo-rheology measurements. Rheological studies were carried out to examine the viscosity of the compositions compared to commercially used bioinks to determine the usefulness of extrusion, where viscosity is of key importance in determining the printing parameters. The results of the FT-IR analyses are shown in Fig. 13.

Investigations into the kinetics of the photopolymerization of highly viscous photocurable compositions have shown that initiating systems with photosensitizers in the form of fluorophores derived from citric acid significantly improve the kinetics and quality of materials prepared using photochemical methods. Both systems are characterized by high efficiency and short induction times. Although a much higher final conversion value was obtained with the **TPA** fluorophore-based system, which would allow more efficient crosslinking of the structure in a shorter period of time, compositions containing both initiating systems were used to further investigate printing possibilities.

The aim of the viscosity tests was to compare the compositions of the commercially available bioinks to determine their initial feasibility for printing and to pre-define the printing parameters. Both compositions developed in this study have very similar viscosity values, but are lower than that of the commercial bioink CELLINK START. For both compositions, the viscosity exceeded 2500 mPa s. Therefore, it was concluded that they were suitable for extrusion-based printing. In this case, the differences between the developed compositions and the commercial bioink should be considered when adjusting the printing parameters.

3.9 3D printing experiments

The final stage of the research was to fabricate 3D printouts of the tested photocurable compositions to assess their potential in 3D printing and the resolution of the structures obtained in this manner. Stereolithography (SLA) 3D printing was the first photochemical technique chosen to produce three-dimensional structures. Images of prints made using a composition containing 70 wt% **PEGDA** and 30 wt% distilled water and an initiating system consisting of 0.1 wt% **CCA** and 1.0 wt% **IOD** are shown in Fig. 14, while prints made from a similar composition only changing the fluorophore to **TPA** as a photosensitizer are shown in the ESI in Fig. S55.†

The 3D printouts obtained with the SLA technique, using a compact device dedicated to the production of small structures, are characterized by a relatively good resolution. The lack of visible pixels on the printout surface may be because of the use of a hydrogel composition containing water, whereby

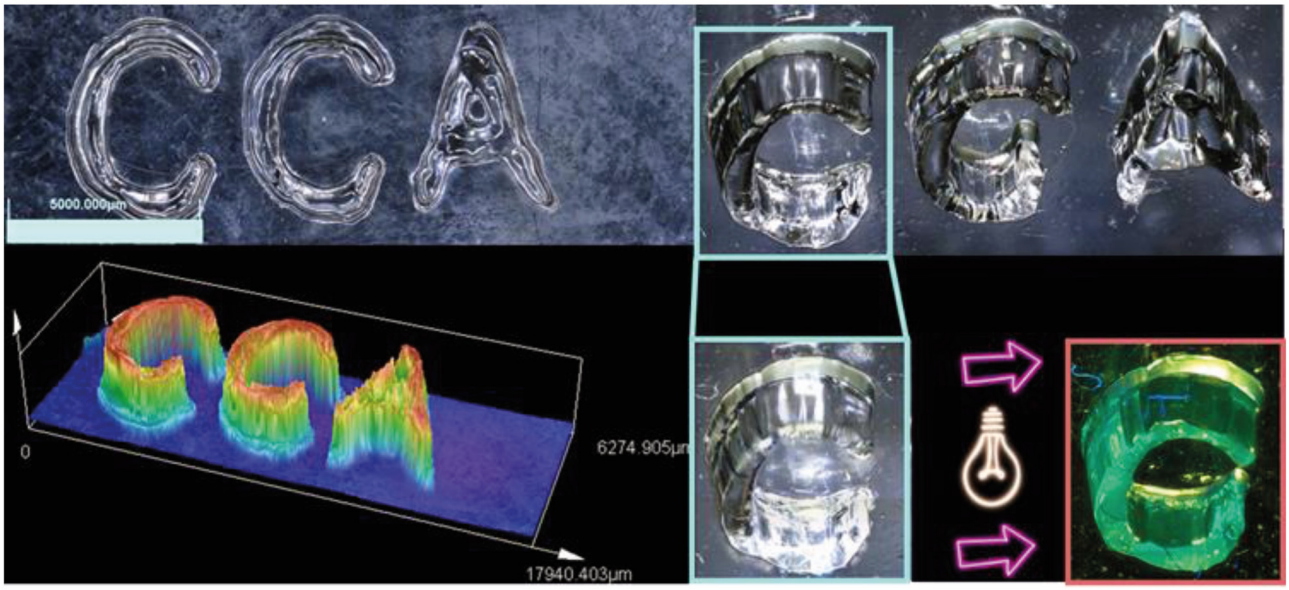

Fig. 13 Microscopic images of obtained 3D prints manufactured using laser engraver printer machine (NEJE DK-8-KZ) equipped with a laser of a wavelength of 405 nm and intensity of 1500 mW using a composition consisting of poly(ethylene glycol)diacrylate (70 wt%) and water (30 wt%). The photoinitiating system consisted of (1.0 wt%) of **IOD** and (0.1 wt%) of **CCA** fluorophore.

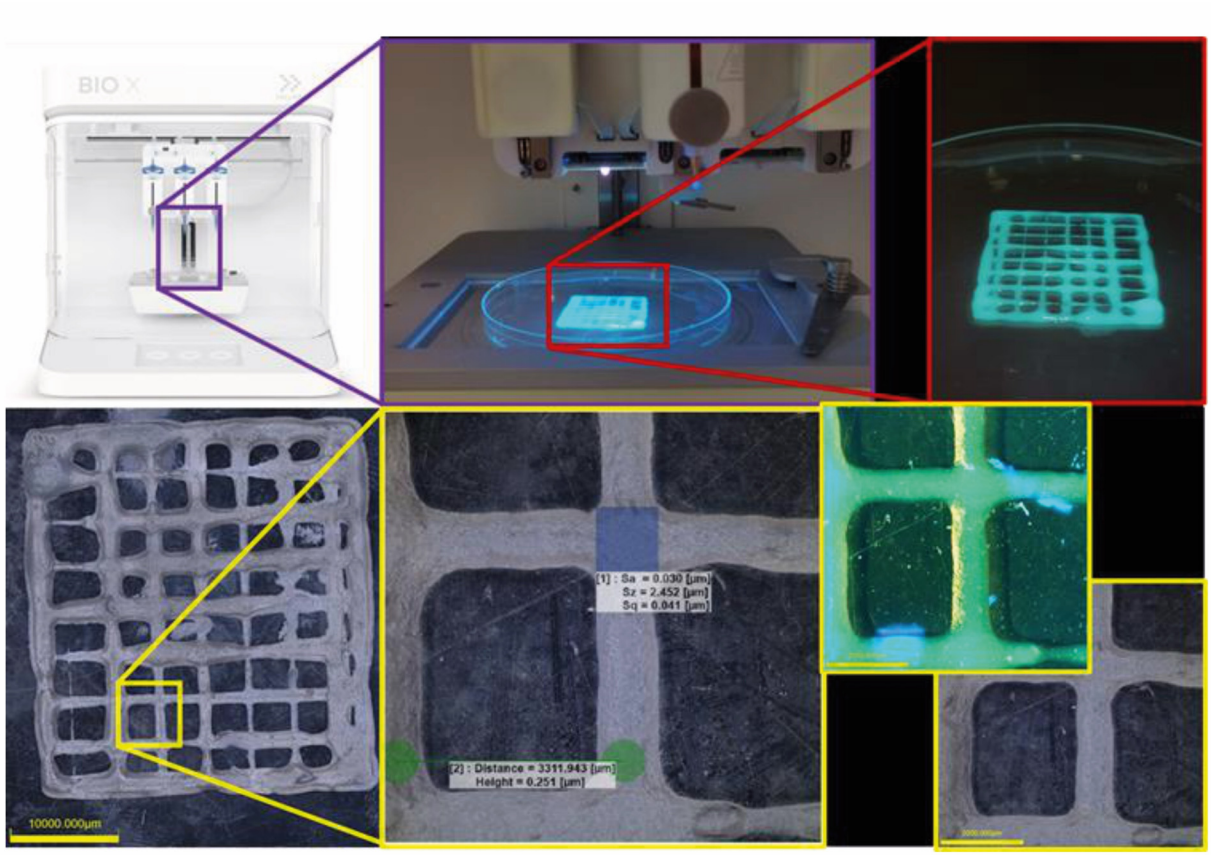

Fig. 14 Microscopic images of obtained 3D prints manufactured using BioX™ printer equipped with a diode of a wavelength of 405 nm and intensity at the sample of 9.88 mW cm^{-2} using a composition consisting of poly(ethylene glycol)diacrylate (70 wt%) and poly(ethylene glycol) (30 wt%). The photoinitiating system consisted of (1.0 wt%) of **IOD** and (0.1 wt%) of **CCA** fluorophore.

the composition is diluted with a non-reactive component. The latter may lead to the migration of polymer chains formed during the printing process, thus affecting the irregularities and subtle curvatures of the plane surface that are visible in the images. The printouts also show good resolution at the bottom layer contacting the glass, which is very promising considering the high light penetration depth of the sample, as evidenced by printout heights of 2.23 mm for the printout with the 0.1 wt% **CCA** and 1.0 wt% **IOD** initiating system and 1.91 mm for the printout with the 0.1 wt% **TPA** and 1.0 wt% **IOD** initiating system.

An additional investigated printing technique was DIW (direct ink writting), which was intended to show another potential application of the developed initiating systems, which, using a resin with appropriate rheological parameters, would allow a completely different type of material, allowing for possible cell cultivation to be obtained. Images of the resulting material for a composition containing 70 wt% **PEGDA**, 30 wt% **PEG**, and an initiating system consisting of 0.1 wt% **CCA** and 1.0 wt% **IOD** are shown in Fig. 14.

The structures obtained by extrusion were characterized by reasonably good resolution and consistency with the design generated by the 3D bioprinter system. Possible shortcomings could be corrected by changing the **PEG** content; however, in this case, the tests involved using the same **PEGDA** oligomer content only with a change in the type of non-reactive component. As regards the resolution of the prints obtained using the DIW 3D printing method, the viscosity and homogeneity of the photo-curable composition play a major role here, which, for the purposes of determining the suitability of the investigated initiating system, was definitely sufficient. However, when it comes to developing the matrix composition of the photo-curable composition, a number of studies would need to be conducted to find the right parameters for both the resin and the print. Regarding the usability of the initiating system, after cross-linking of the extruded structure, all lines present in the structure were fully cured during 120 s of illumination with a diode with a wavelength of 405 nm and an intensity of 9.88 mW cm^{-2}. The structure exhibited good resolution, and most importantly, from the point of view of the research carried out in this study, the initiating system tested worked well for the cross-linking of the finished 3D structures. One conclusion that can already be drawn at this stage is that it is possible to use the investigated derivatives as initiating systems for 3D bioprinting to obtain porous structures on which cells can be deposited. However, it is crucial to further elaborate the composition in terms of monomer/oligomer and non-reactive components.

4. Conclusions

Within the scope of this article, four fluorophores derived from citric acid-based synthesis were investigated, specifically 5-oxo-2,3-dihydro-5*H*-[1,3]thiazolo[3,2-*a*]pyridine-7-carboxylic acid (**CCA**), 5-oxo-2,3-dihydro-5*H*-[1,3]thiazolo[3,2-*a*]pyridine-3,7-dicarboxylic acid (**TPA**), 6-oxo-3,4-dihydro-2*H*,6*H*-pyrido[2,1-*b*][1, 3]oxazine-8-carboxylic acid (**ODPC**) and 3 [(carboxymethyl)carbamoyl]-5-oxo-2,3-dihydro-5*H*-[1,3]thiazolo[3,2-*a*] pyridine-7-carboxylic acid (**CTPC**). In-depth analyses of the spectroscopic characteristics, electron transfer mechanism investigated by spectroscopic and electrochemical methods, and process kinetics and applicational studies of the developed initiating systems were carried out. From spectroscopic studies, it was possible to make a preliminary determination of the suitability of the investigated compounds for 3D printing because of the broad absorption bandwidth that reaches the visible range. The Gibbs free energy (ΔG) for the electron transfer process was calculated from the electrochemical studies, from which it was possible to determine that ΔG was negative for all compounds; that is, both the oxidation and reduction cycles were thermodynamically acceptable. For both these results and those obtained from the determined average fluorescence lifetimes and quenching of the PL emission spectrum, the chromophore **CCA** showed the best potential as a photosensitizer for diphenyliodonium salt (**IOD**).

The hypothesis put forward in this way was confirmed by photopolymerization kinetics studies, where an initiating system containing this photosensitizer allowed the highest final conversion values to be achieved compared to the others. The **ODPC** derivative also showed great potential for possible application in the first stage of the study but was found to be the least effective during kinetics testing. Given the structure of this compound, which is the only one with an oxazine ring instead of a thiazole ring, this suggests that the electron transfer process should occur with lower efficiency. **TPA** and **CTPC** derivatives, on the other hand, when used in the study of kinetics in photocurable resins, showed significantly better properties and higher efficiency in catalyzing the initiation process than the initial analyses suggested. The electrochemical, absorption, and fluorescence results may be influenced by the number and type of substituents in the structure in these two cases. The **CTPC** and **TPA** derivatives, compared to the one for which the lowest value was obtained, were distinguished by the presence of two electron acceptor carboxyl groups. The presence of such groups may negatively affect the electrochemical properties, which may explain why they have higher G values than the other fluorophores during the oxidation cycle. In addition, the complexity of the structure can negatively affect the obtained values.

However, investigations into the kinetics and rheological properties of the material have enabled the selection of suitable initiating systems for use in 3D printing as well as the determination of the composition in terms of the content of the non-reactive component (water). In this case, the aim was to maintain the highest possible dilution, best final conversion results, shortest gel time, and lowest possible shrinkage. Therefore compositions consisting of 70 wt% **PEGDA**, 30 wt% distilled water and an initiating system consisting of 0.1 wt% **CCA** or **TPA**, respectively, and 1.0 wt% **IOD** were selected. The objects obtained from the 3D printing tests using the SLA technique had a good resolution, particularly given the small size

of the overall object. Therefore, these compounds are suitable photosensitizers for initiating systems dedicated to 3D printing of hydrogel structures.

An additional aim of this study was to determine the possibility of using the developed initiating systems in 3D bioprinting based on material pressure extrusion, that is, the DIW technique. To this end, photocurable compositions were developed with appropriate viscosity using the same initiation systems as in previous studies. **PEG** was used as a non-reactive component to alter the rheological properties of the tested formulations. Based on FTIR, classical rheology, and photorheology analyses, it was possible to determine the initial print parameters. The obtained structures were characterized by very good resolution and excellent back-crosslinking, demonstrating that the developed systems can be used to cure thicker layers of materials, such as those produced during extrusion printing.

The main and most important finding of this study is that the tested fluorophores can be successfully used in initiating systems operating in the ultraviolet and visible light ranges dedicated to 3D SLA printing and 3D DIW bioprinting. Photoinitiating systems containing the proposed photosensitizers show significantly higher efficiencies than iodonium salt references and open up the possibility of using these materials for a wide range of applications.

Author contributions

K. S. conceptualization; data curation; validation; methodology; investigation; formal analysis; writing – original draft; writing – review and editing; A. W. organic synthesis; data curation; validation; writing – original draft; writing – review and editing; L. W. organic synthesis; validation; data curation; P. S. computational chemistry; data curation; validation; W. K. organic synthesis; conceptualization; investigation; methodology; supervision; validation; writing – original draft; writing – review and editing; J. O. conceptualization; funding acquisition; investigation; methodology; supervision; validation; writing – original draft; writing – review and editing.

Data availability

The data supporting this article have been included as a part of ESI.†

Conflicts of interest

The authors declare no conflict of interest.

Acknowledgements

This research was funded by the NCN project OPUS ("Emerging strategy approaches for the design and functionalization of carbon dots as multifunctional, dynamic, green systems photoinitiators and photocatalysts involved in photopolymerisation processes"), grant no. UMO-2021/41/B/ST5/04533.

References

1 M. Kaur and A. K. Srivastava, Photopolymerization: A review, *J. Macromol. Sci., Polym. Rev.*, 2002, **42**, 481–512.
2 Y. Li, X. Zhang, X. Zhang, Y. Zhang and D. Hou, Recent Progress of the Vat Photopolymerization Technique in Tissue Engineering: A Brief Review of Mechanisms, Methods, Materials, and Applications, *Polymers*, 2023, **15**, 3940.
3 J. Ortyl, P. Fiedor, A. Chachaj-Brekiesz, M. Pilch, E. Hola and M. Galek, The Applicability of 2-amino-4,6-diphenylpyridine-3-carbonitrile Sensors for Monitoring Different Types of Photopolymerization Processes and Acceleration of Cationic and Free-Radical Photopolymerization Under Near UV Light, *Sensors*, 2019, **19**, 1668.
4 F. Petko, M. Galek, E. Hola, M. Topa-Skwarczyńska, W. Tomal, M. Jankowska, *et al.*, Symmetric Iodonium Salts Based on Benzylidene as One-Component Photoinitiators for Applications in 3D Printing, *Chem. Mater.*, 2022, **34**, 10077–10092.
5 M. Lang, S. Hirner, F. Wiesbrock and P. Fuchs, A Review on Modeling Cure Kinetics and Mechanisms of Photopolymerization, *Polymers*, 2022, **14**, 2074.
6 E. Hola, M. Pilch and J. Ortyl, Thioxanthone Derivatives as a New Class of Organic Photocatalysts for Photopolymerisation Processes and the 3D Printing of Photocurable Resins under Visible Light, *Catalysts*, 2020, **10**, 903.
7 K. D. Jandt and R. W. Mills, A brief history of LED photopolymerization, *Dent. Mater.*, 2013, **29**, 605–617.
8 P. Prabhakaran and K. S. Lee, *Photo-polymerization*, 2019, pp. 1–52.
9 J. Ortyl, P. Milart and R. Popielarz, Applicability of aminophthalimide probes for monitoring and acceleration of cationic photopolymerization of epoxides, *Polym. Test.*, 2013, **32**, 708–715.
10 F. Petko, A. Świeży and J. Ortyl, Photoinitiating systems and kinetics of frontal photopolymerization processes – the prospects for efficient preparation of composites and thick 3D structures, *Polym. Chem.*, 2021, **12**, 4593–4612.
11 A. Ribas-Massonis, M. Cicujano, J. Duran, E. Besalú and A. Poater, Free-Radical Photopolymerization for Curing Products for Refinish Coatings Market, *Polymers*, 2022, **14**, 2856.
12 J. Ortyl, M. Galica, R. Popielarz and D. Bogdał, Application of a carbazole derivative as a spectroscopic fluorescent probe for real time monitoring of cationic photopolymerization, *Pol. J. Chem. Technol.*, 2014, **16**, 75–80.
13 E. Andrzejewska, Free-radical photopolymerization of multifunctional monomers, in *Three-Dimensional Microfabr Using Two-phot Polym*, 2020, pp. 77–99.

14 D. Nowak, J. Ortyl, I. Kamińska-Borek, K. Kukuła, M. Topa and R. Popielarz, Photopolymerization of hybrid monomers, Part II: Determination of relative quantum efficiency of selected photoinitiators in cationic and free-radical polymerization of hybrid monomers, *Polym. Test.*, 2018, **67**, 144–150.

15 J. Wu, Z. Zhao, C. M. Hamel, X. Mu, X. Kuang, Z. Guo, *et al.*, Evolution of material properties during free radical photopolymerization, *J. Mech. Phys. Solids*, 2018, **112**, 25–49.

16 K. Kim, J. Sinha, G. Gao, K. K. Childress, S. M. Sartor, A. M. Salazar, *et al.*, High-Efficiency Radical Photopolymerization Enhanced by Autonomous Dark Cure, *Macromolecules*, 2020, **53**, 5034–5046.

17 J. Ortyl, M. Galek, P. Milart and R. Popielarz, Aminophthalimide probes for monitoring of cationic photopolymerization by fluorescence probe technology and their effect on the polymerization kinetics, *Polym. Test.*, 2012, **31**, 466–473.

18 B. Li, H. Yang, J. He, S. Yu, R. Xiao, H. Luo, *et al.*, Photopolymerization of Coating Materials for Protection against Carbon Steel Corrosion, *Materials*, 2023, **16**, 2015.

19 I. V. Khudyakov, Fast photopolymerization of acrylate coatings: Achievements and problems, *Prog. Org. Coat.*, 2018, **121**, 151–159.

20 M. Topa, J. Ortyl, A. Chachaj-Brekiesz, I. Kamińska-Borek, M. Pilch and R. Popielarz, Applicability of samarium(III) complexes for the role of luminescent molecular sensors for monitoring progress of photopolymerization processes and control of the thickness of polymer coatings, *Spectrochim. Acta, Part A*, 2018, **199**, 430–440.

21 M. T. Islam, A. Dominguez, R. S. Turley, H. Kim, K. A. Sultana, M. A. I. Shuvo, *et al.*, Development of photocatalytic paint based on TiO2 and photopolymer resin for the degradation of organic pollutants in water, *Sci. Total Environ.*, 2020, **704**, 135406.

22 D. Y. Kim, K. M. Lee, T. J. White and K. U. Jeong, Cholesteric liquid crystal paints: in situ photopolymerization of helicoidally stacked multilayer nanostructures for flexible broadband mirrors, *NPG Asia Mater.*, 2018, **10**, 1061–1068.

23 V. Daniloska, P. Carretero, R. Tomovska and J. M. Asua, High performance pressure sensitive adhesives by miniemulsion photopolymerization in a continuous tubular reactor, *Polymer*, 2014, **55**, 5050–5056.

24 V. Besse, M. A. Derbanne, T. N. Pham, W. D. Cook and L. Le Pluart, Photopolymerization study and adhesive properties of self-etch adhesives containing bis(acyl)phosphine oxide initiator, *Dent. Mater.*, 2016, **32**, 561–569.

25 Z. Czech, A. Kowalczyk, J. Ortyl and J. Swiderska, Acrylic pressure-sensitive adhesives containing SiO_2 nanoparticles, *Pol. J. Chem. Technol.*, 2013, **15**, 12–14.

26 M. Topa and J. Ortyl, Moving Towards a Finer Way of Light-Cured Resin-Based Restorative Dental Materials: Recent Advances in Photoinitiating Systems Based on Iodonium Salts, *Materials*, 2020, **13**, 4093.

27 M. Topa-Skwarczyńska, M. Jankowska, A. Gruchała-Hałat, F. Petko, M. Galek and J. Ortyl, High-performance photoinitiating systems for new generation dental fillings, *Dent. Mater.*, 2023, **39**, 729–742.

28 X. Xu, A. Awad, P. Robles-Martinez, S. Gaisford, A. Goyanes and A. W. Basit, Vat photopolymerization 3D printing for advanced drug delivery and medical device applications, *J. Controlled Release*, 2021, **329**, 743–757.

29 P. Patel, K. Dhal, R. Gupta, K. Tappa, F. J. Rybicki, P. Ravi, *et al.*, Medical 3D Printing Using Desktop Inverted Vat Photopolymerization: Background, Clinical Applications, and Challenges, *Bioengineering*, 2023, **10**, 782.

30 G. Pitzanti and D. A. Lamprou, *Vat Photopolymerization Methods for Drug Delivery Applications*, 2023, pp. 181–194.

31 P. Wang, J. Li, J. Yang, G. Wang, L. He and H. Zhang, Enabling 3D multilayer electronics through the hybrid of vat photopolymerization and laser-activated selective metallization, *Addit. Manuf.*, 2023, **74**, 103717.

32 J. G. Kloosterboer, Network formation by chain crosslinking photopolymerization and its applications in electronics, *Electron. Appl.*, 1988, 1–61.

33 P. Wang, J. Li, G. Wang, L. He, J. Yang, C. Zhang, *et al.*, Hybrid additive manufacturing based on vat photopolymerization and laser-activated selective metallization for three-dimensional conformal electronics, *Addit. Manuf.*, 2023, **63**, 103388.

34 S. Doran, O. S. Taskin, M. A. Tasdelen and Y. Yağci, Controlled Photopolymerization and Novel Architectures, *Dyes Chromophores Polym. Sci.*, 2015, 81–121.

35 A. Al Rashid, W. Ahmed, M. Y. Khalid and M. Koç, Vat photopolymerization of polymers and polymer composites: Processes and applications, *Addit. Manuf.*, 2021, **47**, 102279.

36 H. Samadian, H. Maleki, Z. Allahyari and M. Jaymand, Natural polymers-based light-induced hydrogels: Promising biomaterials for biomedical applications, *Coord. Chem. Rev.*, 2020, **420**, 213432.

37 D. Czachor-Jadacka, B. Pilch-Pitera, M. Kisiel and J. Gumieniak, Hydrophobic UV-Curable Powder Clear Coatings: Study on the Synthesis of New Crosslinking Agents Based on Raw Materials Derived from Renewable Sources, *Materials*, 2021, **14**, 4710.

38 A. Bagheri and J. Jin, Photopolymerization in 3D Printing, *ACS Appl. Polym. Mater.*, 2019, **1**, 593–611.

39 W. Tomal, A. Chachaj-Brekiesz, R. Popielarz and J. Ortyl, Multifunctional biphenyl derivatives as photosensitisers in various types of photopolymerization processes, including IPN formation, 3D printing of photocurable multiwalled carbon nanotubes (MWCNTs) fluorescent composites, *RSC Adv.*, 2020, **10**, 32162–32182.

40 F. Petko, M. Galek, E. Hola, R. Popielarz and J. Ortyl, One-Component Cationic Photoinitiators from Tunable Benzylidene Scaffolds for 3D Printing Applications, *Macromolecules*, 2021, **54**, 7070–7087.

41 A. Kafle, E. Luis, R. Silwal, H. M. Pan, P. L. Shrestha and A. K. Bastola, 3D/4D Printing of Polymers: Fused

Deposition Modelling (FDM), Selective Laser Sintering (SLS), and Stereolithography (SLA), *Polymers*, 2021, **13**, 3101.

42 W. Tomal, H. C. Kiliclar, P. Fiedor, J. Ortyl and Y. Yagci, Visible Light Induced High Resolution and Swift 3D Printing System by Halogen Atom Transfer, *Macromol. Rapid Commun.*, 2023, **44**, 2200661.

43 C. J. Li and P. T. Anastas, Green Chemistry: present and future, *Chem. Soc. Rev.*, 2012, **41**, 1413–1414.

44 F. I. Saldívar-González, B. A. Pilón-Jiménez and J. L. Medina-Franco, Chemical space of naturally occurring compounds, *Phys. Sci. Rev.*, 2019, **4**, 20180103.

45 I. Chiulan, E. B. Heggset, Ş. I. Voicu and G. Chinga-Carrasco, Photopolymerization of bio-based polymers in a biomedical engineering perspective, *Biomacromolecules*, 2021, **22**, 1795–1814.

46 A. Mishra and S. Daswal, Curcumin, a natural colorant as initiator for photopolymerization of styrene: Kinetics and mechanism, *Colloid Polym. Sci.*, 2007, **285**, 1109–1117.

47 X. Peng, D. Zhu and P. Xiao, Naphthoquinone derivatives: Naturally derived molecules as blue-light-sensitive photoinitiators of photopolymerization, *Eur. Polym. J.*, 2020, **127**, 109569.

48 C. J. Li and B. M. Trost, Green chemistry for chemical synthesis, *Proc. Natl. Acad. Sci. U. S. A.*, 2008, **105**, 13197–13202.

49 C. Vazquez-Martel, P. Mainik and E. Blasco, Natural and Naturally Derived Photoinitiating Systems for Light-Based 3D Printing, *Org. Mater.*, 2022, **4**, 281–291.

50 M. A. Tehfe, F. Louradour, J. Lalevée and J. P. Fouassier, Photopolymerization Reactions: On the Way to a Green and Sustainable Chemistry, *Appl. Sci.*, 2013, **3**, 490–514.

51 X. Zhang, M. Jiang, N. Niu, Z. Chen, S. Li, S. Liu, *et al.*, Natural-Product-Derived Carbon Dots: From Natural Products to Functional Materials, *ChemSusChem*, 2018, **11**, 11–2447.

52 W. Kasprzyk, T. Świergosz and F. Koper, Fluorescence assay for the determination of d-panthenol based on novel ring-fused 2-pyridone derivative, *Int. J. Mol. Sci.*, 2020, **21**, 1–12.

53 Y. Xiong, J. Schneider, E. V. Ushakova and A. L. Rogach, Influence of molecular fluorophores on the research field of chemically synthesized carbon dots, *Nano Today*, 2018, **23**, 124–139.

54 D. Qu and Z. Sun, The formation mechanism and fluorophores of carbon dots synthesized via a bottom-up route, *Mater. Chem. Front.*, 2020, **4**, 400–420.

55 W. Kasprzyk, T. Świergosz, S. Bednarz, K. Walas, N. V. Bashmakova and D. Bogdał, Luminescence phenomena of carbon dots derived from citric acid and urea – a molecular insight, *Nanoscale*, 2018, **10**, 13889–13894.

56 W. Kasprzyk, T. Świergosz, P. P. Romańczyk, J. Feldmann and J. K. Stolarczyk, The role of molecular fluorophores in the photoluminescence of carbon dots derived from citric acid: current state-of-the-art and future perspectives, *Nanoscale*, 2022, **14**, 14368–14384.

57 L. Placer, L. Estévez, I. Lavilla, F. Pena-Pereira and C. Bendicho, Assessing citric acid-derived luminescent probes for pH and ammonia sensing: A comprehensive experimental and theoretical study, *Anal. Chim. Acta*, 2021, **1186**, 339125.

58 M. Schäferling, Nanoparticle-based luminescent probes for intracellular sensing and imaging of pH, *Wiley Interdiscip. Rev.:Nanomed. Nanobiotechnol.*, 2016, **8**, 378–413.

59 L. Di Costanzo, B. Panunzi, R. J. Pieters, T. Terai, E. Yavin, A. Samhan-Arias, *et al.*, Visual pH Sensors: From a Chemical Perspective to New Bioengineered Materials, *Molecules*, 2021, **26**, 2952.

60 H. O. Othman, F. Salehnia, M. Hosseini, R. Hassan, A. Faizullah and M. R. Ganjali, Fluorescence immunoassay based on nitrogen doped carbon dots for the detection of human nuclear matrix protein NMP22 as biomarker for early stage diagnosis of bladder cancer, *Microchem. J.*, 2020, **157**, 104966.

61 M. Tian, R. Wu, C. Xiang, G. Niu and W. Guan, Recent Advances in Fluorescent Probes for Cancer Biomarker Detection, *Molecules*, 2024, **29**, 1168.

62 X. Yao, R. E. Lewis and C. L. Haynes, Synthesis Processes, Photoluminescence Mechanism, and, the Toxicity of Amorphous or Polymeric Carbon Dots, *Acc. Chem. Res.*, 2022, **55**, 3312–3321.

63 J. D. Stachowska, A. Murphy, C. Mellor, D. Fernandes, E. N. Gibbons, M. J. Krysmann, *et al.*, A rich gallery of carbon dots based photoluminescent suspensions and powders derived by citric acid/urea, *Sci. Rep.*, 2021, **11**, 10554.

64 K. Muthamma, D. Sunil and P. Shetty, Carbon dots as emerging luminophores in security inks for anti-counterfeit applications - An up-to-date review, *Appl. Mater. Today*, 2021, **23**, 101050.

65 A. Abdollahi, H. Roghani-Mamaqani, B. Razavi and M. Salami-Kalajahi, Photoluminescent and chromic nanomaterials for anticounterfeiting technologies: Recent advances and future challenges, *ACS Nano*, 2020, **14**, 14417–14492.

66 M. K. Barman and A. Patra, Current status and prospects on chemical structure driven photoluminescence behaviour of carbon dots, *J. Photochem. Photobiol., C*, 2018, **37**, 1–22.

67 Z. Wang, X. Xiao, T. Zou, Y. Yang, X. Xing, R. Zhao, *et al.* Citric Acid Capped CdS Quantum Dots for Fluorescence Detection of Copper Ions (II) in Aqueous Solution, *Nanomaterials*, 2019, **9**, 32.

68 D. Shan, J. T. Hsieh, X. Bai and J. Yang, Citrate-Based Fluorescent Biomaterials, *Adv. Healthcare Mater.*, 2018, **7**, 1800532.

69 F. Yan, X. Sun, F. Zu, Z. Bai, Y. Jiang, K. Fan, *et al.*, Fluorescent probes for detecting cysteine, *Methods Appl. Fluoresc.*, 2018, **6**, 042001.

70 H. Feng, J. Liu, A. Qaitoon, Q. Meng, Y. Sultanbawa, Z. Zhang, *et al.*, Responsive small-molecule luminescence

probes for sulfite/bisulfite detection in food samples, *TrAC, Trends Anal. Chem.*, 2021, **136**, 116199.

71 A. H. Loo, Z. Sofer, D. Bouša, P. Ulbrich, A. Bonanni and M. Pumera, Carboxylic Carbon Quantum Dots as a Fluorescent Sensing Platform for DNA Detection, *ACS Appl. Mater. Interfaces*, 2016, **8**, 1951–1957.

72 L. Placer, I. Lavilla, F. Pena-Pereira and C. Bendicho, Bromine speciation by a paper-based sensor integrated with a citric acid/cysteamine fluorescent probe and smartphone detection, *Sens. Actuators, B*, 2022, **358**, 131499.

73 W. Kasprzyk, S. Bednarz, P. Zmudzki, M. Galica and D. Bogdał, Novel efficient fluorophores synthesized from citric acid, *RSC Adv.*, 2015, **5**, 34795–34799.

74 W. Tomal, T. Świergosz, M. Pilch, W. Kasprzyk and J. Ortyl, New horizons for carbon dots: quantum nano-photoinitiating catalysts for cationic photopolymerization and three-dimensional (3D) printing under visible light, *Polym. Chem.*, 2021, **12**, 3661–3676.

75 E. Andrzejewska, D. Zych-Tomkowiak, M. Andrzejewski, G. L. Hug and B. Marciniak, Heteroaromatic thiols as co-initiators for type II photoinitiating systems based on camphorquinone and isopropylthioxanthone, *Macromolecules*, 2006, **39**, 3777–3785.

76 P. P. Romańczyk and S. S. Kurek, The Reduction Potential of Diphenyliodonium Polymerisation Photoinitiator Is Not −0.2 V vs. SCE. A Computational Study, *Electrochim. Acta*, 2017, **255**, 482–485.

77 B. Strehmel, Application of NIR-photopolymers in the graphic industry: From physical chemistry to lithographic applications, *Z. Phys. Chem.*, 2014, **228**, 129–153.